C00-4308-1

LASER MATERIALS

CONTRACT NO. ES-77-C-02-4308

JULY 1, 1977 TO JULY 31, 1978

SANDERS ASSOCIATES, INC.

95 CANAL STREET

NASHUA, N. H.

AUGUST 8, 1979

PREPARED FOR:

THE DEPARTMENT OF ENERGY

OFFICE OF INERTIAL CONFINEMENT FUSION

DISCLAIMER

ABSTRACT

Fluoride materials display specific properties applicable for use as active and passive optical elements for advanced laser programs. Generally, these materials exhibit low values of n_2 and high ultra violet transmission. Nd:YLF is a very promising laser fusion oscillator element operating in conjunction with phosphate and fluoroberyllate systems. New materials possessing high concentrations of terbium and cerium - KTb_3F_{10}, $RbTb_3F_{10}$ and potassium cerium compounds, display high magneto-optical rotatory power, high Verdet's constant, for use as faraday rotators. Requirements for these materials for use in laser fusion power plants include large aperture; initial growth scaling issues for fluoride crystals were addressed. A study was conducted to improve the efficiency of fluoride lasers. The proposed system employs a rare gas halide excimer laser to pumped specific energy levels of the solid state component thus yielding a high efficiency storage laser.

Nd:YLF, operating at 1.047 μm or 1.053 μm has been identified as the most promising oscillator material for phosphate and fluoroberyllate systems. Crystal growth parameters were optimized and neodymium dopant levels of about 1% in the lattice were achieved during this program. Excellent optical quality material was grown at a rate of .5mm/hr. Melt circulation was improved through increased furnace thermal gradients and reduced seed-rod rotation rate. Laser rods fabricated during this program were mode-locked at the Lawrence Livermore Laboratory, and the University of Rochester Lab for Laser Energetics.

The new materials investigation included crystal growth and phase study of KTb_3F_{10}. KTb_3F_{10} displays one of the highest figures of merit of any known material. Preliminary growth studies of other potential rotator materials included the $RbF\text{-}Tb_3F_{10}$ and the $KF\text{-}CeF_3$ systems. Compounds of both systems are expected to display high Verdet's constants.

Furnace design and parametric design for growth of larger fluoride crystals were considered. A heat zone for growth of 70mm crystals was fabricated.

A study was conducted to investigate the use of rare gas halide excimer lasers in conjunction with solid state lasers to design a high efficiency, low heat loading, solid state storage laser system suitable for use as inertial confinement fusion drivers. Three candidates were identified: XeF pumped Tm:YLF emitting at 450 nm, XeF pumped Nd:YLF emitting at 360 nm or 380 nm, and KrF pumped Ho:YLF emitting at 249 nm.

PREFACE

This is a report of an investigation of crystalline fluoride materials intended for application for laser fusion. The investigation was funded by the Department of Energy under Contract No. E.S.-77-C-02-4308, laser materials. The period covered in this report is 1 July 1977 to 31 July 1978.

Dr. Joel Weis and Dr. Paul Hoff, Office of Inertial Confinement Fusion, were technical monitors to this program.

These studies were performed by the Advanced Technology Department, Defensive Systems Division of Sanders Associates, Inc.. The Crystal Physics Laboratory, Department of Electrical Engineering and Center for Materials Science, Massachusetts Institute of Technology served as Subcontractor. Mr. Robert C. Folweiler was principal investigator at Sanders and the program coordinator. Mr. Evan P. Chicklis assisted Mr. Folweiler in this program. Mr. Chicklis conducted the study of rare gas halide pumped solid state storage lasers. Mr. Folweiler was assisted by Mr. Thomas Pollak in the crystal growth of Nd:YLF. Technical functions of crystal growth, fabrication and optical analysis at Sanders were done by Philip Foley and Leo Terrenzio.

The work at the Crystal Physics Laboratory is under the direction of Dr. A. Linz, and includes growth of new materials, feed synthesis and spectroscopy. Dr. David Gabbe performed the crystal growth, and the feed material process development and synthesis. Dr. Hans Jenssen performed the spectroscopic measurements.

TABLE OF CONTENTS

FIGURES

TABLES

1.0 INTRODUCTION AND SUMMARY

1.1 Introduction

This final report describes work performed by Sanders Associates for the Department of Energy under Contract No. E.S-77-C-02-4308, Laser Materials. The objectives of this program were to conduct research and development on crystalline optical materials suitable for propagation of the high peak powers associated with laser fusion research, and to investigate the feasibility of resonant pumped solid state storage lasers as advanced devices for inertial confinement fusion experiments.

The materials research portion of the program focused on growth and characterization of crystalline fluoride materials. These materials as a class have certain generalized properties-such as low n_2 and high ultraviolet transmission-which are desirable for many applications in D.O.E.'s advanced laser program. Specifically, Nd:YLF and KTb_3F_{10} have very desirable properties for certain fusion applications. The tasks in this portion of the program were to:

- Grow and fabricate Nd^{+3} doped $LiYF_4$ laser rods suitable for operation in a master oscillator.
- Maximize Nd^{+3} concentration in YLF, exhibiting a distribution coefficient of .38.
- Determine the suitability of Nd:YLF as an oscillator material for laser fusion.
- Grow crystals of new cubic rare earth fluorides, particularly $K(RE)_3F_{10}$, and determine the pertinent properties.
- Improve the material processing for crystal growth, in particular the hydrofluorinating process of raw materials.

The resonant pumped laser investigation portion of the program focused on identifying solid state laser systems which might be capable of exhibiting the performance necessary for power plant applications (efficiency and scaleability). Solid state laser materials have certain inherent properties which render them useful in laser fusion experiments. These properties include high storage densities, long storage times, appropriate stimulated emission cross-sections, a wide diversity of optical transitions in the .3 - 3 μm region and, host materials with low n_2. Many solid state materials have previously been rejected for power plant applications due to low overall efficiency and high thermal loading. These phenomena would lead to optical distortion and/or material failure. In a resonant pumped laser, the fraction of the pump radiation absorbed, hence the laser efficiency can be made very high. By choosing the pump level close to the upper laser level, the heat input can be made quite low. For high system efficiency, it is necessary to choose pump lasers which are scaleable to high energies and average powers and which operate with high overall efficiency. ArF, KrF, and XeF rare gas halide excimer lasers have shown potential for 50-100 kj per laser with wall plug efficiencies between 5-15%.

In this program, Sanders investigated the applicability of solid state laser materials as storage media for ArF, KrF, and XeF pumps. The specific program objectives were:

- To identify potential storage laser media with absorption at the pump laser lines.
- To identify systems with relaxation modes consistent with low thermal input.
- To model the thermal processes.
- To perform spectroscopic measurements of candidate transitions.
- To initiate resonant pumping experiments.

The program was conducted by Sanders Associates in conjunction with its subcontractor, Massachusetts Institute of Technology.

1.2 Summary

The highlights of the program are summarized below:

- Nd:YLF has been identified as the most promising oscillator material for phosphate [1] and fluoroberyllate [2] systems. Excellent optical quality material has been delivered and laser rods have been mode-locked at Lawrence Livermore Laboratories, and at the Laboratory for Laser Energetics of the University of Rochester. This laser material has been transitioned to a commercial product.

- Growth of Nd:YLF with 3% neodymium in the melt, yielding ~ 1% in the crystal has been accomplished. This concentration is comparable to Nd:YAG.

- Samples of KTb_3F_{10} have been grown and a partial phase diagram developed. This cubic Faraday rotator material exhibits a 4.3 times higher figure of merit than FR-5.

- $RbTb_3F_{10}$ has been identified as a potential high figure of merit rotator material. Preliminary data indicates that this material is a congruently melting compound, a property which facilitates scale of the growth.

- The $KF-CeF_3$ system has been investigated as Ce^{+3} ion has almost the same rotatory power as Tb^{+3} at a lower cost. Preliminary study of the phase diagram was begun.

- Investigation into growth of large fluoride crystals has begun. A larger hot zone to grow up to 70mm diameter crystals was designed and purchased, including a 1000 cm^3 platinum crucible.

- A survey of rare-earth doped and transition metal ion doped solids has revealed several candidates suitable for resonant pumping by Rare Gas Halide (RGH) excimer lasers.

- In specific instances, very high efficiencies with very low heat deposition appear likely in RGH pumped solid state (storage) lasers.

- The best candidate systems appear to be XeF pumped Tm^{3+}:YLF emitting at 450 nm, XeF pumped Nd:YLF emitting at 360 or 380 nm, and KrF pumped Ho^{3+}:YLF emitting at 249 nm. In all cases, it is estimated that the fractional heat loading is less than 10% of the stored energy.

- The absorption cross section of Tm^{3+}:YLF at at 353 nm (XeF) is $\sigma_A = 6 \times 10^{-22}$, the stimulated emission cross section of the $D_2 \rightarrow {}^3H_4$ transition is 6-9 x 10^{-20} cm^2. The ${}^1D_2 \rightarrow {}^3H_4$ emission peaks at 451 nm and its relaxation appears to be nearly 100% radiative with a room temperature lifetime of 67 μs (1% Tm). A heat loading of ~10% (or less) of the extractable energy appears possible in XeF pumped Tm^{3+}:YLF. Growth of 10% Tm^{3+}:YLF is underway.

- Nd^{3+}:YLF exhibits an absorption cross section of 1.4×10^{-20} cm^2 at 353 nm. Emission is observed from the pump multiplet (believed to be $^4D_{3/2}$) at 353 to $^4I_{9/2}$ (364 nm), $^4I_{11/2}$ (382 nm), $^4I_{13/2}$ (410 nm), and $^4I_{15/2}$ (450 nm). Determination of fluorescence branching rations, non radiative decay rates, and emission cross sections is presently underway.

- The absorption cross section of Ho^{3+}:YLF at 249 nm (KrF) is $\sim 4 \times 10^{-22}$ cm^2. Insufficient data is available currently for quantitative heat loading estimates under KrF pumping.

- Cr^{3+}:Al_2O_3, because of its superb physical properties and its favorable spectroscopic properties,will be an excellent candidate if efficient RGH pumps in the 550 nm region are developed. Because of the high absorption cross section in this region, very low Cr^{3+} concentrations (lower than in ruby) would be appropriate and crystalline quality comparable to sapphire might be obtainable.

2.0 MATERIALS

2.1 Growth of Nd:YLF

2.1.1 Introduction

Four crystal growth runs and experiments were performed to improve the growth process of Nd:YLF. Increased growth rates were attempted by altering compensating growth parameters. Laser rods were fabricated from boules grown during this program, delivered to selected laboratories, and were successfully mode locked by several investigators [1, 2, 3, 5, 6]. The neodymium doping level in the laser crystals were approximately the same as used in Nd:YAG ($\sim$1%). This was desirable to increase the energy output. Growth parameters were altered considerably to accommodate the increased concentration of neodymium.

2.1.2 Growth Run Data

The initial growth experiment was performed to attempt to increase the growth rate of Nd:YLF. Further growth runs attempted and successfully introduced a nominal $\sim$1% neodymium in the tetragonal lattice of YLF.

2.1.2.1 Growth of Boule 526f

Growth rate evaluation was made during this experiment. Raw materials consisted of Research Chemicals YF_3, purified NdF_3 from M.I.T. and LiF from Hawshaw Chemicals. The boule was seeded and widened using normal procedure, and then grown under diameter control at different pulling rates, starting at 0.5 mm/hr and increasing to 2.0 mm/hr. Between 5 and 29 mm were grown at each rate, with the results shown in Table 1. The growth rate was dropped to the lowest rate for the last segment to ascertain whether the defects were driven by impurity build-up in the melt or simply by the pulling

TABLE 1

EFFECT OF GROWTH RATE ON Nd:YLF

$Li\ Y_{0.975}\ Nd_{0.025}\ F_4$

BOULE #526

SEED ROTATION 10 RPM

PULL RATE mm/hr	LENGTH mm	COMMENTS
0.5	5	Clear, no detectable defects
0.8	22	Clear, no detectable defects
1.2	17	Clear, no detectable defects
1.6	29	Light haze in center, increasing size as crystal grew
2.0	12	Increased defect size; occupies most most of diameter
0.5	10	Clear, no detectable defects

rate. Since the resultant growth was clear, we concluded that the defects are pull rate driven. From this experiment, we concluded that a growth rate of 1.0 mm/hr is acceptable, and will be used for future growth runs. Figure 1 illustrates boule #526F grown during this experiment.

The increased growth rate is a result of changes in two of the parameters in our furnace:

1. Decreased rotational speed
2. Increased thermal gradient

Decreased rotational speed was used in conjunction with the increased thermal gradient to change the crystal/melt interface conditions. The combination changed the circulation pattern at the base of the crystal so that the interface ceased to act as a centrifugal pump, and circulation is now radially inward over most of the interface in contrast to radially outward over most of the interface. The latter condition reduced mixing over the center portion of the crystal, undoubtedly leading to constitutional super-cooling and internal defects. There still appears to be a central zone of reverse flow, but it is much smaller and defects appear only at the higher pull rates. The increased thermal gradient was obtained by lowering the crucible from its position at the top of the hot zone, so that it is entirely within the hot zone. This makes the top of the melt hotter. These changes were discovered and applied to growth runs to successfully grow boules free of radial strain.

2.1.2.2 Growth of Boule 528C

Purified material was used for this growth run containing 3% neodymium in the melt to introduce 1% neodymium into the crystal. A growth rate of 1.0 mm/hr was used.

One kilogram of 6-9's Y_2O_3 was bought from Research

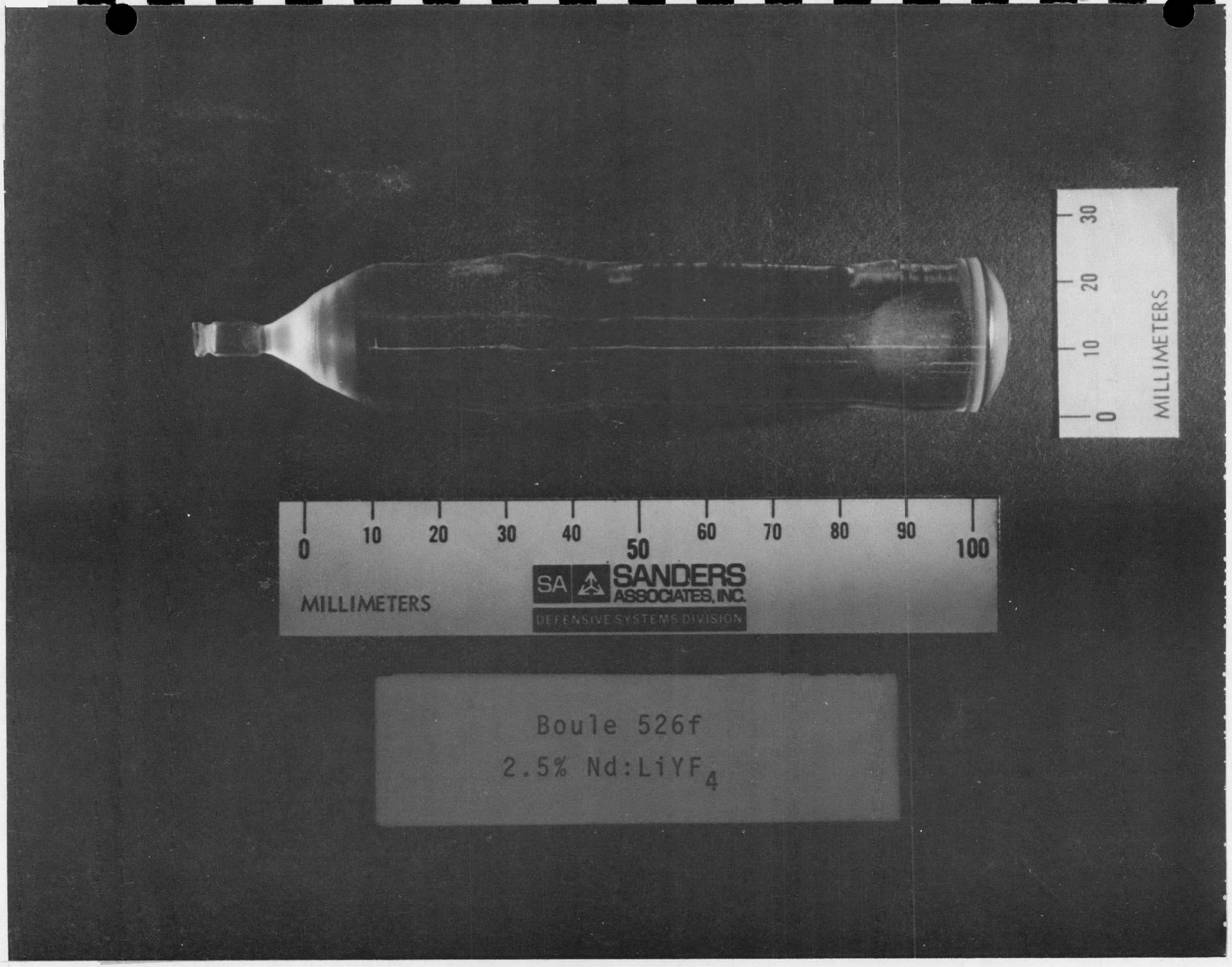
0
10
20
30
40
50
60
70
80
90
100
MILLIMETERS
SA
SANDERS
ASSOCIATES, INC.
DEFENSIVE SYSTEMS DIVISION
0
10
20
30
MILLIMETERS
Boule 526f
2.5% Nd:LiYF4

FIGURE 1

Chemical, Inc. to be purified and processed into YF_3 via $Y_2(CO_3)_3$. Eleven hundred grams of slightly wet $Y_2(CO_3)_3.2.3\ H_2O$ has been hydrofluorinated. The remaining carbonate has been synthesized and was washed and filtered before hydrofluorination.

The commercial Y_2O_3 was dissolved in hydrochloric acid forming a neutral solution of YCl_3. A blue insoluble residue remained and was removed by filtration. Transition metal impurities were precipitated with diethylammonium diethyl-dithiocarbamte (DDDC) and removed by filtration through a 0.2 μm polycarbonate medium.

The filtrate was tested and found to contain a small amount of transition metal impurity not removed in the previous step. Several extrations with DDDC in $CHCl_3$ and oxine in DDDC were done. The chelate precipitate as well as the chloroform extracts have been saved for analysis.

Yttrium chloride hexahydrate was precipitated from this purified chloride solution by saturating with HCl gas.

The purified $YCl_3.6H_2O$ was dissolved in a solution of urea purified by mixed ion exchange and 0.2 μm filtration. This filtration was hydrolyzed at 95-100°C under CO_2 pressure to form $Y_2(CO_3)_3.2.3\ H_2O$.

During the initial meltdown for growth, a portion of the charge did not melt. Subsequent examination showed the presence of oxyfluoride. The charge was broken up and rehydrofluorinated for an extended period to eliminate the oxyfluoride. When the charge was melted again in the crystal growth furnace, it melted at a lower temperature than usual by approximately 25°C. We have no explanation for this latter observation at the present.

A boule was grown from this melt that weighed 221 g, 26 mm diameter by 110 mm long, Figure 2, a pull rate of 1.0 mm/hr was used. A conical shaped series of scattering sites was found in the grown

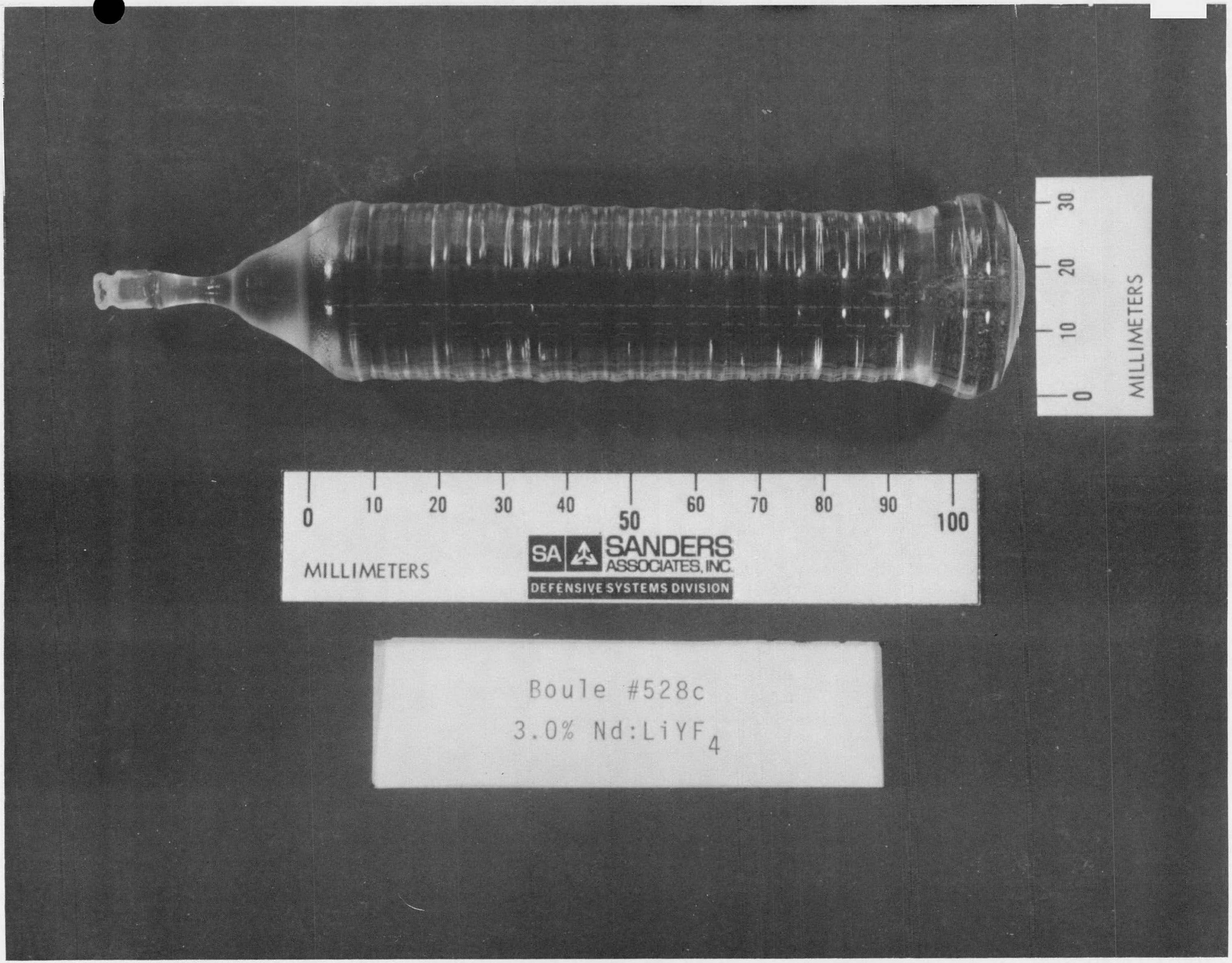
0 10 20 30 40 50 60 70 80 90 100
MILLIMETERS
SA SANDERS ASSOCIATES, INC.
DEFENSIVE SYSTEMS DIVISION
0 10 20 30
MILLIMETERS
Boule #528c
3.0% Nd:LiYF4

FIGURE 2

crystal, with its apex near the top, preventing fabrication of usable laser rods. The next boule will be grown, using a combination of fresh feed material and boule 528C.

2.1.2.3 Growth of Boule #530

The material for this growth run consisted of fresh purified feed, processed as discussed in the last growth run. Boule 528C was also added to make up the feed. A growth rate of .8 mm/hr was employed.

The growth rate was reduced from 1.0 mm/hr to 0.8 mm/hr to eliminate the scatter centers encountered in the previous run. The inclusion of the additional neodymium in the melt and boule apparently caused the "pull rate" driven defect mechanism to become dominent at a lower growth rate.

Boule #530, pictured in Figure 3, weighed 260.1 gms and measured 25-26 mm in diameter by 118 mm in length. The residual melt weighed 231.0 gm. In viewing a polarometer, it was determined that the boule was polycrystalline in nature. Improper melt-back caused the polycrystalline nature of the boule. Scatter at the core of the boule was also observed, apparently, still related to a too rapid growth rate.

2.1.2.4 Growth of Boule 537

The melt and boule from growth 530 was rehydrofluorinated and used for growth 537. A quality, single crystal boule was grown at a rate of .5 mm/hr. Six laser rods were fabricated and delivered to selected laboratories.

Boule #537 was grown at a rate of .5 mm/hr. The scatter in the boule was almost nonexistant, a section in the center of the bottom did contain a small core.

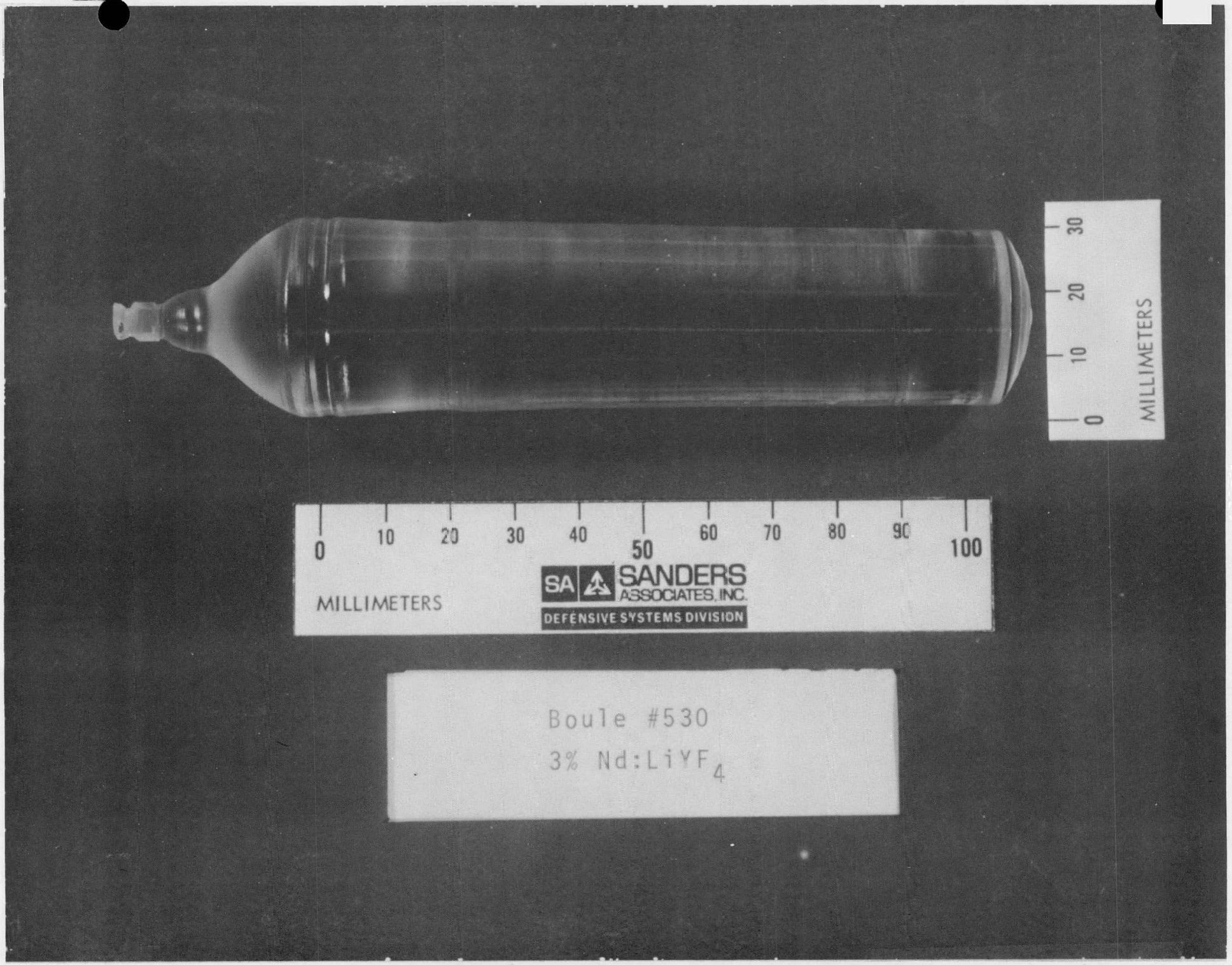
0 10 20 30 40 50 60 70 80 90 100
MILLIMETERS
SA SANDERS ASSOCIATES, INC.
DEFENSIVE SYSTEMS DIVISION
0 10 20 30
MILLIMETERS
Boule #530
3% Nd:LiYF4

FIGURE 3

Boule 537 weighed 279.5 gms, Figure 4. The boule dimensions were 25 mm in diameter by 110 mm in length. The residual melt weighed 164 gms.

Five laser rods were fabricated and delivered to the following laboratories:

John McMahon, NRL

1 rod 6.35 mm in diameter x 76 mm in length. The ends were cut with a Brewster angle for operation at 1.053 mm.

Eric Jones, Sandia Laboratory

Received 2 rods 5.0 mm in diameter by 75 mm in length ends cut flat and parallel.

Wolf Seka, University of Rochester

Received 1 rod, 4.0 mm in diameter by 6.0 mm in length, ends cut flat and parallel; 1 rod 4.0 mm in length by 76 mm in length, the ends were cut 2^{o} and 2.5^{o}, respectively, from the normal to the rod axis.

Representative interferograms are shown in Figures 5 and 6. Path distortion was very minimal in these rods. Rods # 537.1 and 537.4 were delivered to Wolf Seka and John McMahon, respectively.

2.1.3 Evaluation of Nd:YLF Laser Rods

Nd:YLF laser rods fabricated from Sanders single crystal boules have been mode locked by several investigators[1, 2, 3, 5, 6]. The material has output at either 1.053 μm or 1.047 μm by polarization

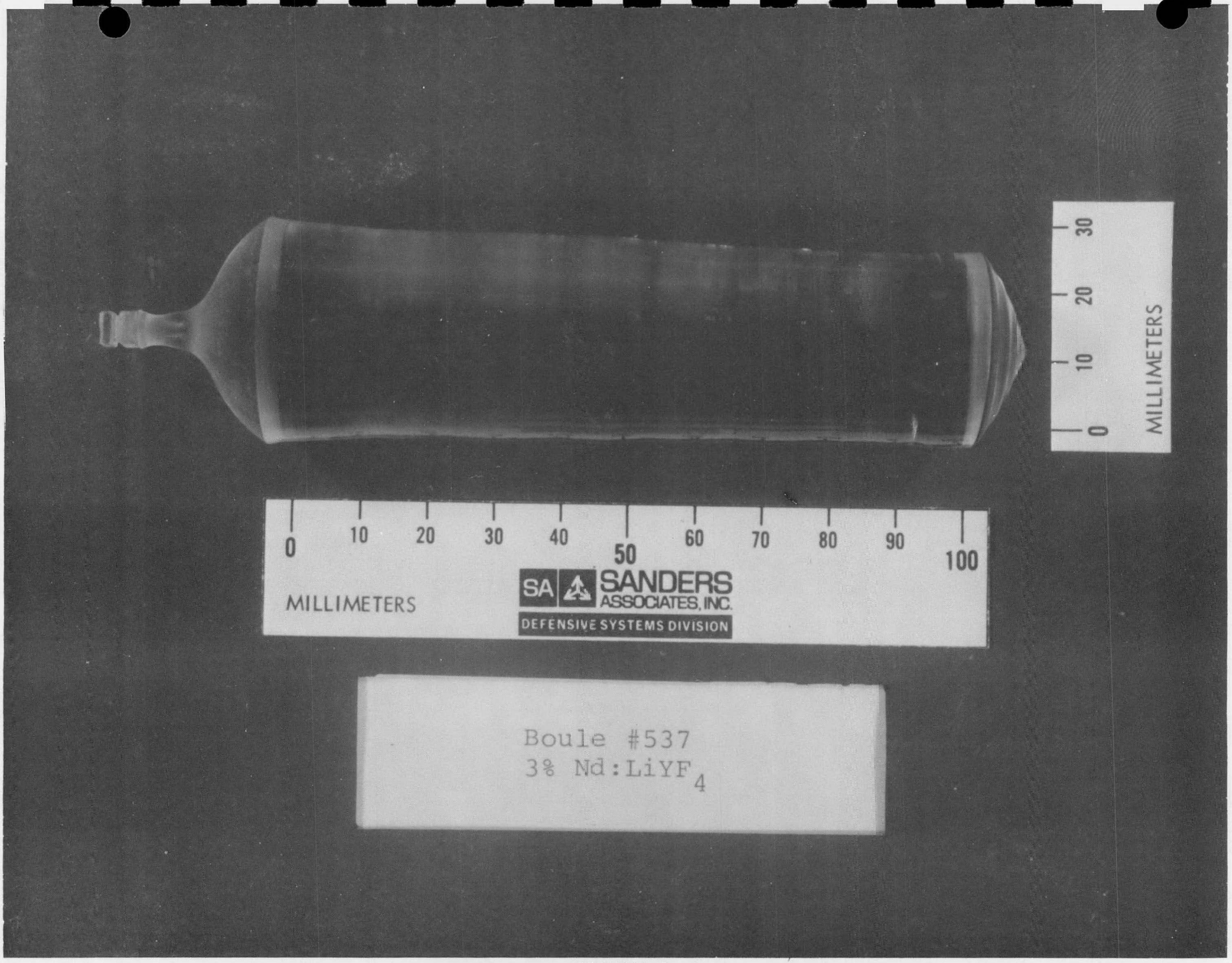
0 10 20 30 40 50 60 70 80 90 100
MILLIMETERS
SA SANDERS ASSOCIATES, INC.
DEFENSIVE SYSTEMS DIVISION
0 10 20 30
MILLIMETERS
Boule #537
3% Nd:LiYF4

FIGURE 4

INTERFEROGRAM OF LASER ROD 537.1

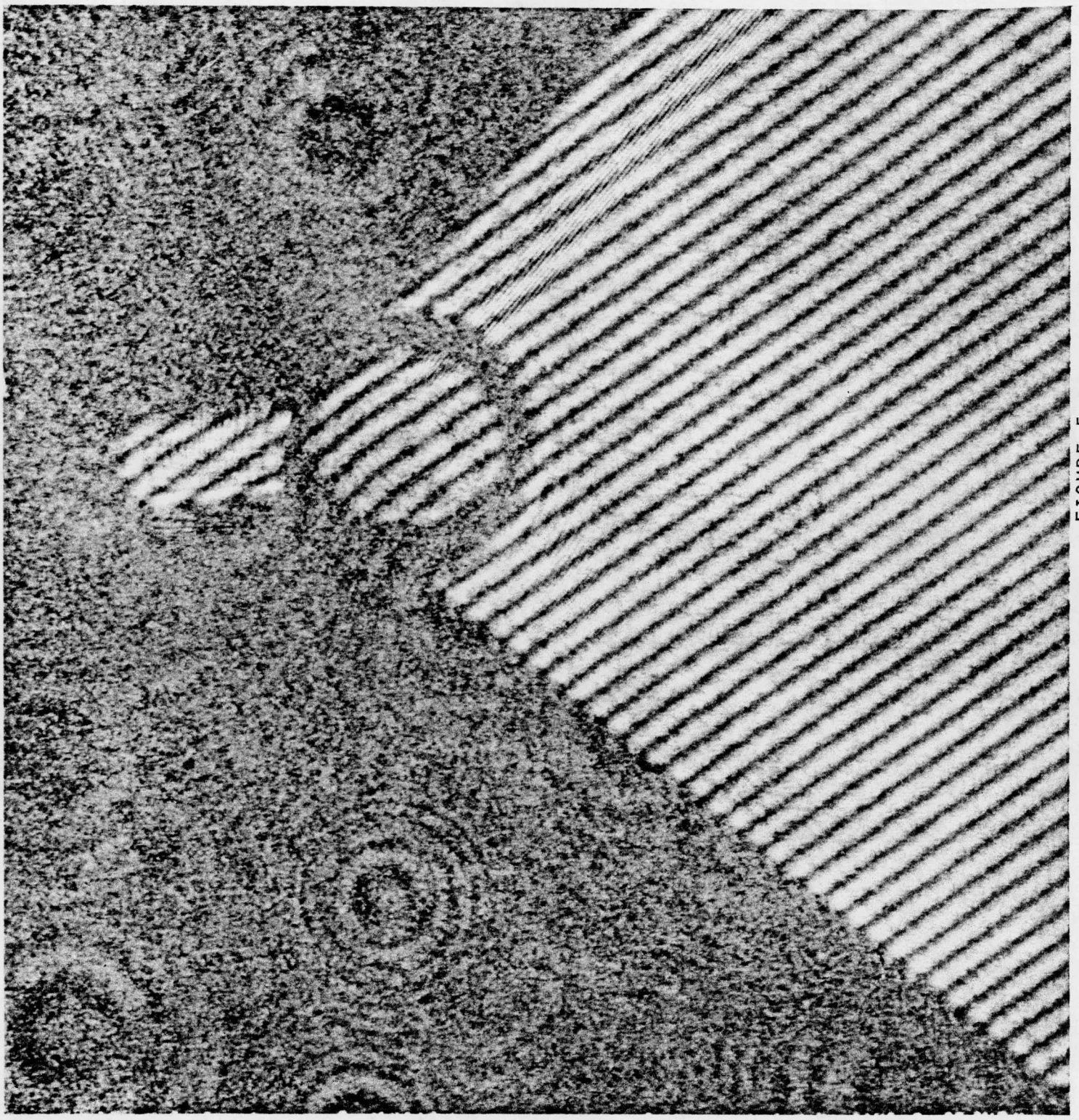

FIGURE 5

INTERFEROGRAM OF LASER ROD 547.4

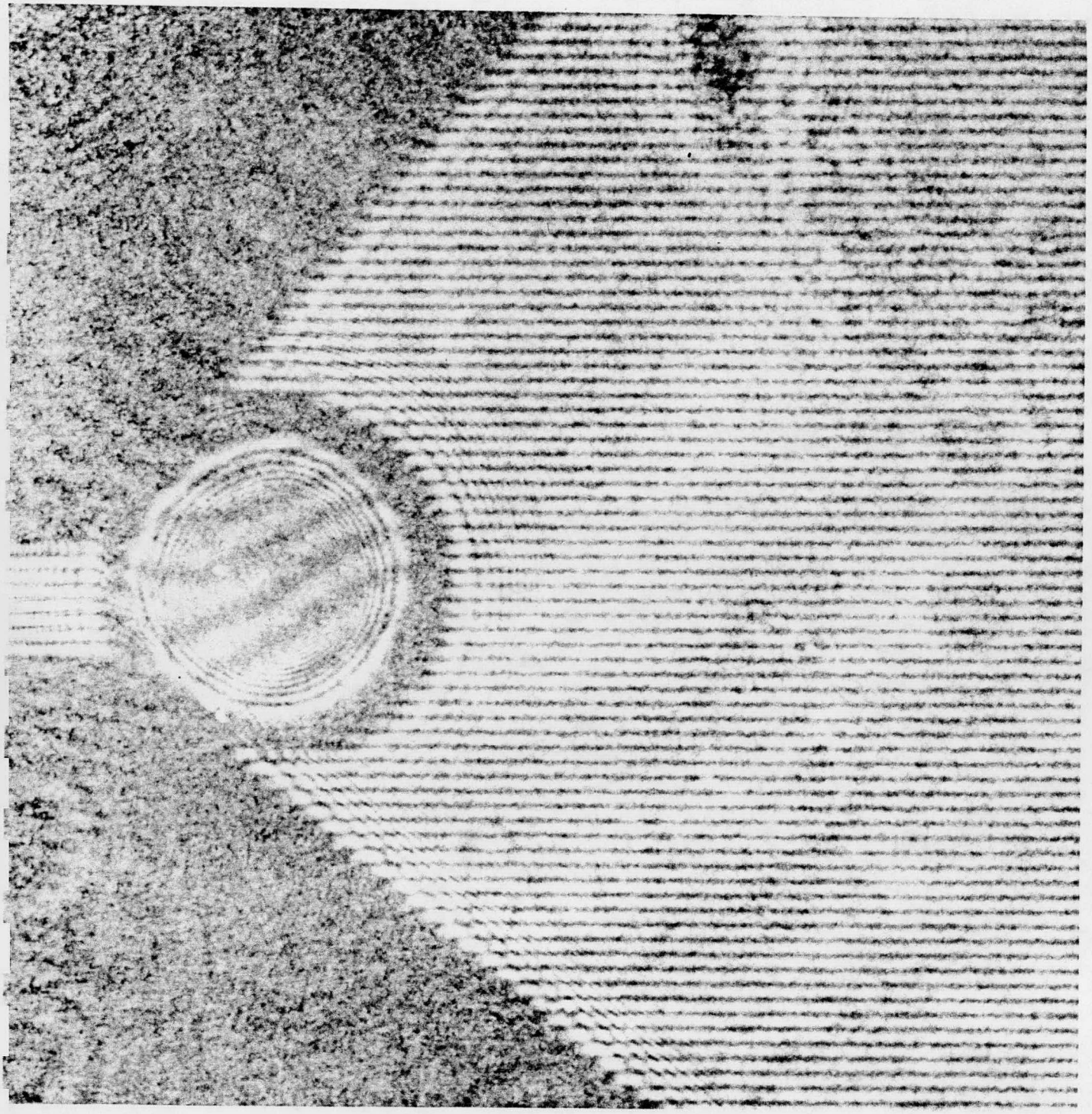

FIGURE 6

selection, and can, therefore, couple into various Nd doped amplifier glasses that are being considered for application in the near future[4]. The stimulated emission cross-section and, therefore, the gain is different, a function of the polarization selection. For π polarization, E vector parallel to the c-axis:

$$\sigma_{EMISSION} = 6.2 \times 10^{-19} \text{ cm}^2.$$

Wavelength output is at 1.047 μm. For σ polarization, E vector perpendicular to the c-axis:

$$\sigma_{EMISSION} = 2.3 \times 10^{-19} \text{ cm}^2$$

Wavelength output is at 1.053 μm.

Q switching of Nd:YLF rods were performed with an active and a passive mechanism [5]. Pulsewidths and cycle times were comparable to Nd:YAG. The threshold was observed to be higher in Nd:YLF than its oxide counterpart at the 1.053 μm.

Nd:YLF was substituted for Nd:YAG in a Q-switch resonator[6]. Similar pulse times were observed, in the region of 3 nanoseconds. Operation with Nd:YLF rods fabricated with Brewster ends oriented for operation at 1.053 μm required an additional Brewster plate filter to suppress operation at 1.037 μm.

2.2 Development of New Materials

2.2.1 The $KF-TbF_3$ System

KTb_3F_{10} is a candidate material for use as Faraday rotator material. Properties of this material and FR-5 glass are shown in Table II. During this program, we have shown KTb_3F_{10} to be incongruently melting, requiring growth from a non-stoichiometric melt with an excess of KF. This only limits the size of the crystal that can be grown from

TABLE II

MEASURED MAGNETO-OPTICAL PROPERTIES OF KTb_3F_{10} AND HOYA'S FR-5 GLASS

	FR-5	KTb_3F_{10}
n (1.06 μm)	1.67	1.50
n_2 (10^{-13} esu)	2.1	0.7 (est)
-V (min/Oe-cm)		
325 nm	1.51	2.16
441 nm	0.63	0.93
633 nm	0.25	0.40
1064 nm	0.071	0.11

a given melt, as is the case with $LiYF_4$ (YLF). In the latter case, where the details of the phase diagram are better known, the maximum mass of the crystal is limited to 95% of the starting melt, more than is suitable for quality crystal growth since impurities concentrate in the melt.

Boules have been grown successfully from a 30 mol % KF - 70 mol % TbF_3 melt, but a subsolidus precipitate has been observed when the crystals were grown from a 35 mol % KF - 65 mol % TbF_3 melt. The precipitate may well be an oxyfluoride phase that has made so much of the reported information on fluoride systems incorrect. The nature of the precipitate is being investigated because it presents a further limit on the amount of quality - KTb_3F_{10} that may be grown from a melt, in addition to the limits placed by the incongruent nature of the phase. We presently anticipate that the usable material from one melt will be on the order of 20% of the initial charge, certainly adequate for the preparation of large boules.

KTb_3F_{10} samples grown under this contract were tested and evaluated at LLL[7]. Table II is a summary of the measured properties of KTb_3F_{10} in comparison to Hoya's FR-5 glass. The measured verdet constant of KTb_3F_{10} is approximately 50% larger than for FR-5, while the estimated n_2 is a factor of 3 smaller. The figure of merit, nV/n_2 for KTb_3F_{10} is 4.3 times that for FR-5. KTb_3F_{10} exhibited a transparent range from 400 to 1500 nm except for a narrow region at about 490 nm.

2.2.2 The $RbF-TbF_3$ System

Compounds in the $RbF-TbF_3$ system are of potential interest as Faraday rotator materials. The larger size of rubidium compared with potassium may simplify the phase equilibria. Vedrine et al[8] report a face centered cubic $RbTb_3F_{10}$ subsolidus phase isostructural with KY_3F_{10} and as expected an isomorphous $RbGd_3F_{10}$ structure. Kozak et al[9], however, report a cubic subsolidus $RbGd_3F_{10}$ with a primitive

cell of 20.44 Å disagreeing with Vedrine's data and implying a disagreement with the data on $RbTb_3F_{10}$. The reported subsolidus instability of $KbTb_3F_{10}$ must be compared with the similar instability reported for KY_3F_{10} which, however, we have shown to be a stable, congruently melting compound.

2.2.3 $KF-CeF_3$ System

This system is of great interest as a magneto-optic rotator since the Ce^{3+} ion has almost the same rotary power as Tb^{3+} and the raw material cost of cerium compounds is much lower than terbium compounds.

Our work in the $KF-REF_3$ [10] systems has indicated that much published data is incorrect. Borzenkova et al [11] report that KY_3F_{10} is stable only in the solid phase, decomposing to two other solid phases before melting takes place. We have grown large single crystals of KY_3F_{10} from a stoichiometric melt. Labeau et al [12] have characterized KEr_3F_{10} as monoclinic. We, however, have grown cubic, congruently melting KEr_3F_{10} by zone refining. Therefore, we chose to reinvestigate some of the features of the CeF_3-KF phase diagram shown in Figure 7 which was determined by Barton et al [13].

A zone refining experiment was done on a charge with a bulk composition of 75 mol % CeF_3 and 25 mol % KF (point A) to establish some features of the phase diagram as well as to crystallize for identification of intermediate phases. Preserved in the zone crystallized ingot is a record of the crystallization path which is interpreted in much the same way as a normal freezing crystallization path. The results of this experiment were at variance with the published phase diagram.

Appearance of single phase CeF_3 at the head of the charge was not observed, whereas Figure 7 suggests that this should occur when the initial system composition is that indicated by point A.

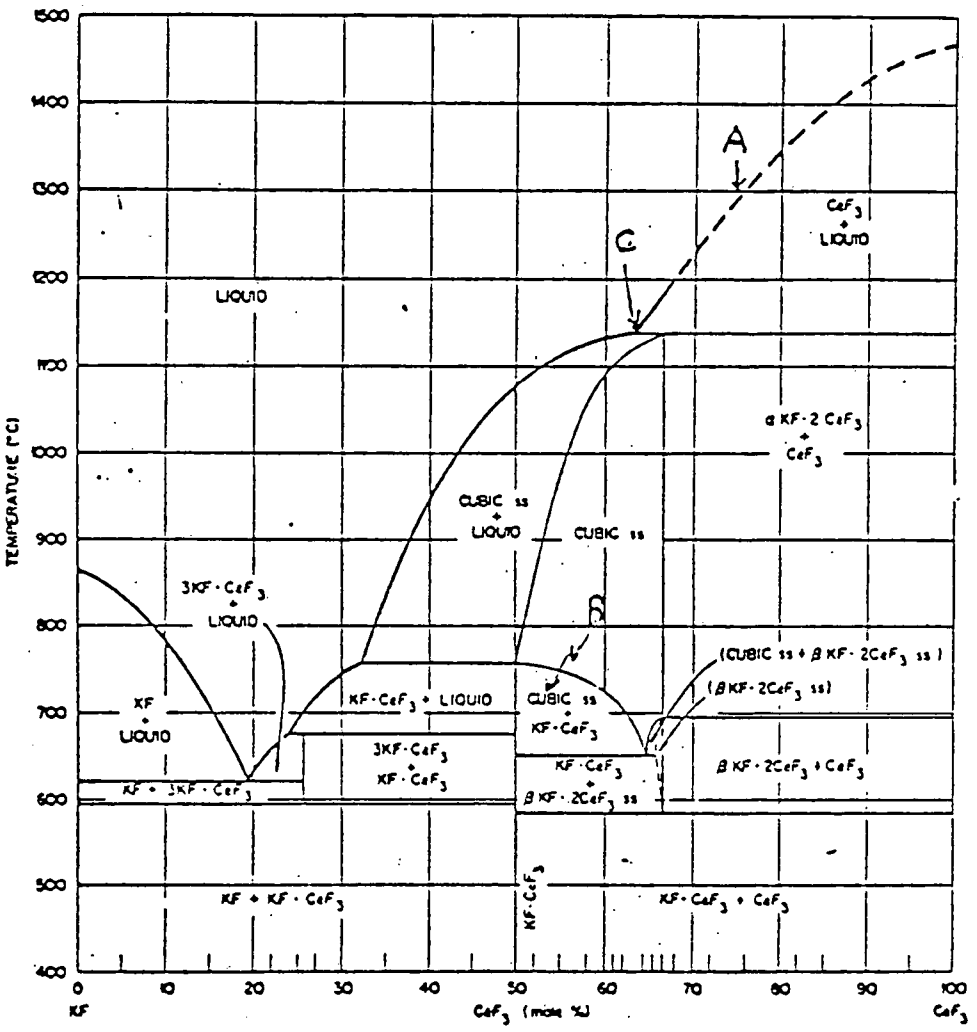

FIGURE 7

KF-CeF_3 SYSTEM

Virtually the whole charge of crystallization was a mixture of very well crystallized (sharp diffraction lines with resolution of CuK_{α_1} and Cu_{α_2}) CeF_3 and a cubic phase. Crystallites were of the order of 0.1 to 0.3 mm in size and not uniformly distributed throughout the volume of the solid mixture. These observations suggest that both phases were co-crystallized directly from the melt rather than formed by decomposition of a solid solution followed by a phase transition as indicated by region B in Figure 7. Peritectic crystallization, C of Figure 7, would yield a well crystallized mixture of CeF_3 and $KF{\cdot}2CeF_3$ at high temperature, but would not persist over the length of the charge, rather being confined to a narrow zone beyond which crystallization along liquidus D would be observed. Thus further investigation of the $KF.CeF_3$ system is needed to establish the existance of useful phases. Additional zone-refining experiments combined with a few single crystal growth experiments at selected melt compositions will serve to characterize the primary phases and the general shape of the liquidus.

2.3 Materials Preparation

New hydrofluorination apparatus has been installed and used for this program. The new apparatus consists of a ceramic tube (99.9% Al_2O_3) lined with 0.25 mm of Pt-10% Rh allow, and a pure platinum (99.99%) boat on a graphite carrier. The reactor tube is closed with flat plates of polytetrafluorethylene (PTFE) backed by water cooled copper plates.

Platinum radiation shields are used in each end of the tube to reduce axial losses and aid in more uniform thermal distribution. The platinum lined apparatus is installed in an existing Sanders owned three zone furnace with an upper temperature limit of 1200°C, which results in a maximum temperature of 1140°C at each end of the platinum boat. Sanders has purchased a new furnace, as yet undelivered that will allow a maximum temperature of 1500°C, 300°C, higher than present.

The new reactor allows direct conversion of the oxides and carbonates to fluorides avoiding the previous two step conversion. The earlier processing approach used a PTFE lined reactor to convert purified carbonate to 99% fluoride at 300°C. This product was then treated at 850°C in a Grafoil lined Inconel reactor, with potential contamination of the feed material during the transfer from the Inconel tube. Our experience to date has demonstrated very favorable results with the new reactor, particularly since most of the rare earth trifluorides may be melted in the apparatus in an atmosphere of HF, improving the conversion rate of the process. Melting of the fluoride reduces the kinetic limitations on the removal of oxygen and oxides that may be present in the feed when compared to solid state reactions on powders.

2.4 Growth of Large Fluoride Crystals

Crystal growth of fluoride crystals to larger diameters has become an important issue. Increased aperture sizes of optical elements, KTb_3F_{10} for Faraday rotators and RE;YLF for resonant pumped lasers, will require growth of crystals up to 200 mm in diameter.

The first growth scaling experiment will be to grow crystals 60 to 70 mm in diameter. A new larger hot zone for the existing furnace has been purchased under the current program, consisting of a new heater of purified graphite, new crucible support, molybdenum heat shields, and a 1000 cm^3 platinum crucible. This larger crucible provides the physical size to grow 70 mm diameter crystals, as well as containing the larger volume of melt required. The new hot zone is illistrated in Figure 8.

The crucible has a diameter of 125 mm. Literature reports of investigation of maximum crystal diameter/crucible diameter ratio suggests that a value of .5 to .6 is suitable for both silicon [14] and gadolinum gallium garnet (GGG) [15] to maintain favorable circulation in the melt.

HOT ZONE FOR GROWTH OF 70mm DIAMETER FLUORIDE CRYSTALS

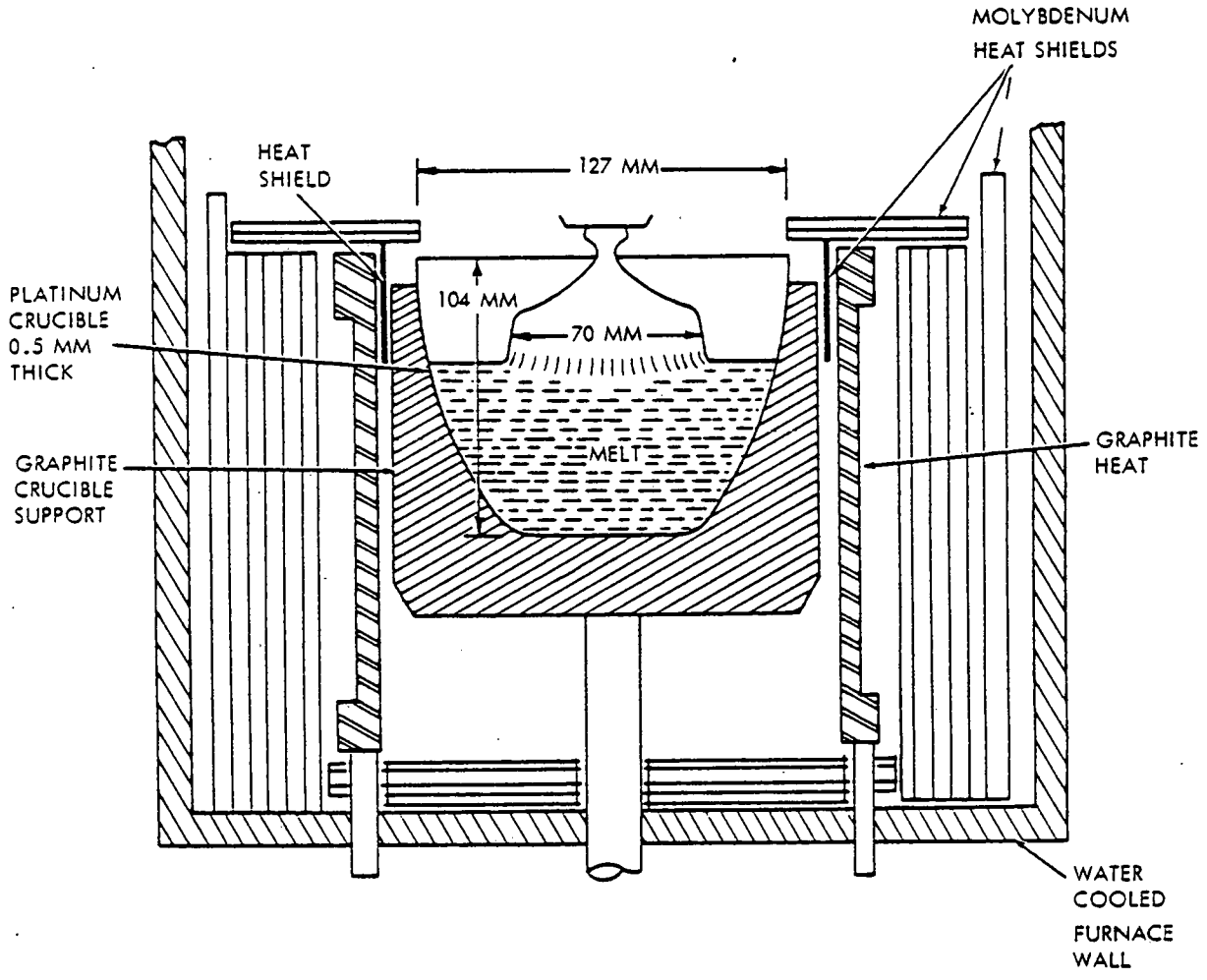

FIGURE 8

Modification of the seed rod design and fabrication of the new seed rod has been completed. The new seed rod was designed with the grow of large crystals in mind. The new design will increase the stability of the growth process by eliminating mechanical vibrations translated to the melt. The stiffness of the seed rod was increased by the following:

- The alloy used was annealed 17-7 pH s.s. rather than 304 s.s.
- The seed rod diameter was increased to 3/4 inch from 5/8 inch of the old design.

Installation of the assembly onto the crystal furnace is in progress at this time.

3.0 RESONANT PUMPED LASER INVESTIGATION

3.1 Background

Solid state laser materials have many desirable properties for laser fusion experiments but had been rejected for power plant applications because of:

1. Low overall efficiency
2. High thermal loading which would lead to optical distortion and/or material failure.

On the other hand, solid state laser materials can exhibit the following very desirable properties:

1. Very high energy storage densities
2. Long storage times and appropriate stimulated emission cross sections
3. A wide diversity of optical transitions in the 0.3 - 3 μm region.
4. Host materials with adequately low n_2.

Furthermore, solid state lasers represent a well developed technology with demonstrated capability of scaling to the required output powers needed for a fusion driver.

The thermal limitations of solid state lasers are associated with the means of excitation. In conventional (lamp-pumped) lasers, the upper laser level is fed by, in general, a series of higher lying narrow pump bands which absorb the pump radiation and then relax to the upper laser level (see Figure 9). In most cases, the relaxation process is multiphonon relaxation, viz, the energy decrement between each pump level and the upper laser level is deposited as heat. Other sources of heat can include direct lattice

FIGURE 9

LASER TYPES

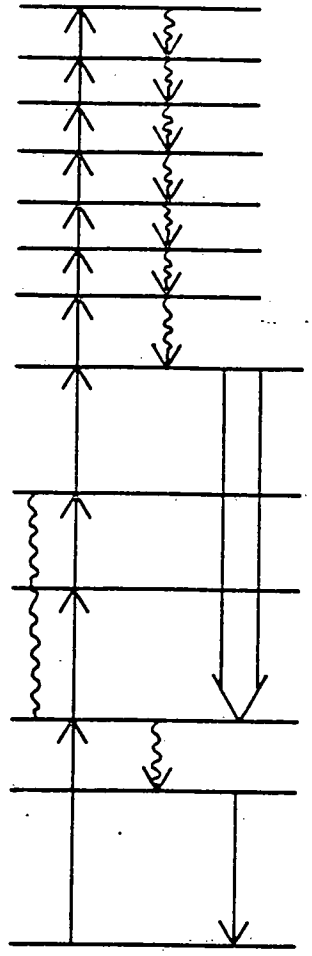

LAMP PUMPED LASER

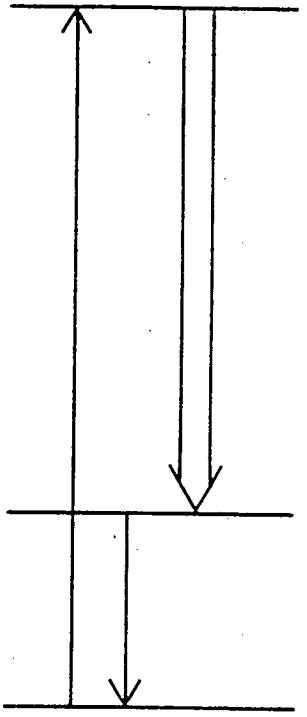

RESONANT PUMPED LASER
(IDEAL)

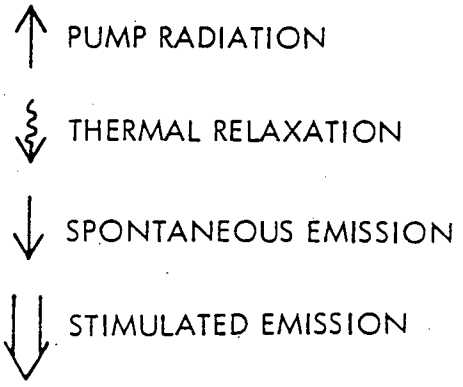

absorption of ultra violet and long wavelength radiation and the excitation of states not directly involved in the laser transition which relax with the emission of phonons.

The efficiency limitations of solids are also associated with the means of excitation. The overlap of the emission of conventional (blackbody) sources with pump band absorption is generally very small. This together with the inefficiencies of optical coupling result in rather low optical pumped laser efficiencies. Resonant pumped lasers, however, can overcome both these deficiencies.

In a resonant pumped laser, the fraction of the pump radiation absorbed, hence the laser efficiency, can be made very high. By choosing the pump level close to the upper laser level the heat input can be made quite low. For high system efficiency, it is necessary to choose pump lasers which are scaleable to high energies and average powers and which operate with high overall efficiency. ArF, KrF, and XeF rare gas halide excimer lasers have shown potential for 50-100 kj per laser with wall plug efficiencies between 5-15%.

On the current program, we have investigated the applicability of solid state laser materials as storage media for ArF, KrF, and XeF pumps. The program methodology has been the:

(a) Identification of potential storage laser media with absorption at the pump laser lines.

(b) Identification of systems with relaxation modes consistent with low thermal input.

(c) Modeling of the thermal processes.

(d) Spectroscopic measurements of candidate transitions.

(e) Initiation of resonant pumping experiments.

In the following parts of this section, we provide:

(a) Idealized models of resonant pumped lasers to identify sources of heat.

(b) A survey of possible resonant pumped laser transitions with their respective estimated heat loads and

(c) Identification of promising storage laser materials and measurement of some of their relevant spectroscopic properties.

3.2 Thermal Modeling

In a well designed flashpumped Nd:YAG laser approximately 1.5 watts of heat are generated in the material per watt of laser output [16]. In a resonant pumped system, the heat load could be much lower since pump band to metastable level relaxation can be minimized. In this section, we model the processes which result in heat loading of resonant pumped lasers.

Sources of heat in optically pumped lasers include:

(a) Pump band to metastable relaxation via multiphonon relaxation.

(b) Terminal level relaxation via multiphonon relaxation.

(c) Direct lattice absorption.

(d) Upconversion and excited state absorption.

(e) Intramanifold relaxation.

By choosing a system carefully (a) can be minimized and (c) eliminated altogether. Relaxation within a manifold (J multiplet for rare earth ions) cannot be eliminated but can be minimized by avoiding the excitation of levels not involved in the specific laser transition.

If we consider only pump band and terminal level relaxation, for the moment, there are means of reducing the heat input. This can be done by choosing:

(a) A system for which the upper laser level is resonant or near resonantly pumped.

(b) A system whose terminal level relaxes by spontaneous emission, stimulated emission, or resonant transfer.

(c) A three level of quasi-3 level system for which terminal level relaxation results in a very small heat input.

We consider specific models below to illustrate these effects.

3.3 Idealized Models

3.3.1 Type I Laser

This system consists of the three levels, shown in the figure below. The pump transition is 1 → 3, the laser transition is

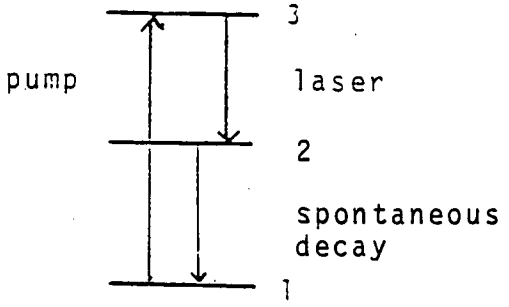

is 3 → 2 and the terminal manifold level relaxation is 2 → 1. In this ideal system, no heat is generated provided the 2 → 1 transition is radiative and that all 3 → 2, 3 → 1 transitions are radiative.

3.3.2 Type II Laser

This system is similar to the Type I laser but more realistic in that the levels are crystal field split levels of J manifolds such as in rare-earth doped crystals. Typical crystal field splitting, might be 300 cm^{-1} in a fluoride host. Electrons in J manifolds are in thermal equilibrium with the lattice.

Radiative transitions between J manifolds occur between individual levels of the upper and lower manifolds. The heat load associated with such a transition depends on the oscillator strengths of the individual levels and their occupation factors. For simplicity we might assume that in any relaxation process between J multiplets the corresponding heat load is equal to the line width of both transitions. This is equivalent to assuming in the diagram below that in the initial state an electron is in the highest level of J_2. It then relaxes to the lowest level of J_2, undergoes a purely radiative transition to the highest level of J, then relaxes to the ground state. The heat load is $Q = \Delta E_2 + \Delta E_1$

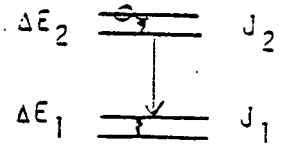

This leads to the type II laser diagrammed below:

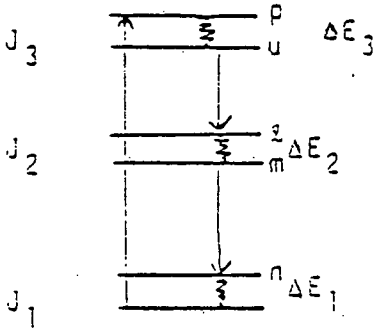

This system is pumped to some upper level p which relaxes through a gap in E_3 to the upper laser level u. The pump level need not be part of J_3 but must be close enough ($\Delta E_3 < 2000\ cm^{-1}$) for rapid multiphonon relaxation. The laser transition is $u \rightarrow \ell$ and the final transition is $m \rightarrow n$. We consider various sub classifications.

3.3.3 Type IIa, All Radiative Transitions

In this use, the $m \rightarrow n$ and $u \rightarrow \ell$ transitions are purely radiative. At first, it would appear that the thermal load is simply

$$\Delta E_1 + \Delta E_2 + \Delta E_3 = Q$$

and the fractional heat load

$$Q' = \frac{Q}{u - \ell}$$

So with typical values of ΔE's for J manifolds of rare-earth ions in fluoride hosts of 300 cm^{-1}, Q = 900 cm^{-1}. For an optical laser transition at 450 nm, E = 22 x 10^3 cm^{-1} and the fractional heat load is only

$$Q' = 4\%$$

The loading would be considerably less if the center of gravity of the J multiplets were used as the u, m, and n states. The assumption here is that p is in the J_3 multiplet.

This model, however, assumes that all the fluorescence leaves the crystal without reabsorption. In any real system reabsorption of the m-n and u-n fluorescence could result in very substantial additional heat input. This effect could be increased still further by trapping of the fluorescence by wall reflections.

If more of the u level population can be extracted by simulated emission u-n fluorescence trapping can be avoided. The heat associated with m-n emission can be minimized by choosing a system with minimal overlap of the $J_2 - J_1$ emission with the $J_1 - J_2$ absorption.

3.3.4 Type IIb

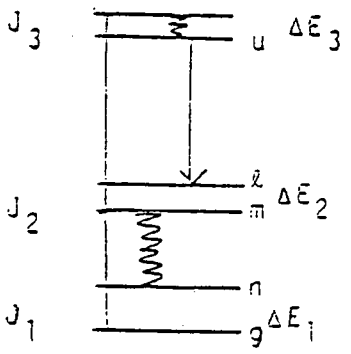

In this model J_2 relaxes by multiphonon relaxation (heat). This model is equivalent to the worst case type IIa system. We assume that the $\ell \rightarrow g$ transitions are purely phonon assisted so that the heat load is

$$Q = \Delta E_3 + \Delta E_2 + \Delta E_1 + |J_2|^*$$

The real world distinction between Type IIa and b depends on the magnitudes of J_2 since multiphonon relaxation rates are energy gap dependent. In fluorides for $|J_2|$ <4000 cm (approximately) Type IIb behavior dominates. For $|J_2|$ >4000 cm, J_2 will relax predominantly by fluorescence, i.e., Type IIa. One of the major advantages of fluoride hosts (compared to oxides) is their lower multiphonon relaxation rates.

---

*$|J_1|$ is the energy above ground of the center of gravity of the i^{th} manifold.

If fluorescence reabsorption is significant, a Type IIb system may be more desirable.

3.3.5 Type IIc

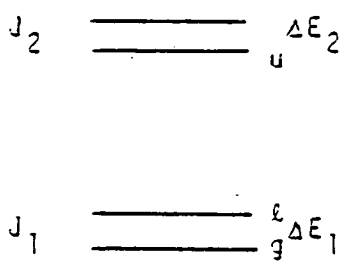

This is a "quasi - 3 level system which for sufficiently large J_2 will quarantee purely radiative transitions. The thermal issue in this system is fluorescence trapping and a practical system would require minimal overlap of fluorescence with the absorption spectrum. Other issues associated with this model are:

(a) E_1 must be significantly larger than kT (200 cm^{-1} at 300K) to minimize the population of the ℓ level.

(b) The output wavelength for reasonable values of E_2 and E_1 (few hundred cm^{-1}) will be very close to the pump wavelength which means uv output for the current pump candidates.

3.3.6 Type III

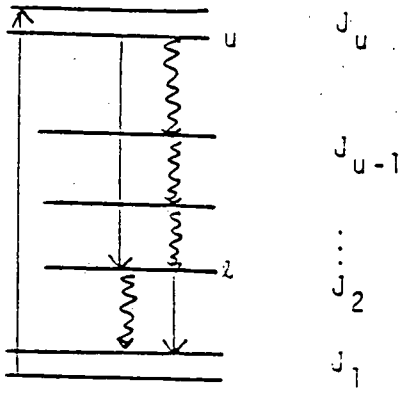

This is a generalized model which resembles most rare-earth ions. The issue here is whether most of the u population can be extracted by stimulated transitions to avoid thermal relaxation between the lower lying J multiplet and other competitive processes. If most of the u level population can be extracted than this system can be approximated by Type IIa or b models. If not, one must account for all other de-excitation modes.

3.4 Specific Candidates

3.4.1 Criteria

At the present time, the most promising pump lasers are ArF, KrF and XeF which emit at 193, 249, and 353 nm respectively. Thus, the first requirement for a high power laser is absorption at the pump line. Other requirements include:

(a) Radiative transitions out of the upper level with a lifetime much longer than the pump pulse (1-10 μs).

(b) Narrow gap between the pump and upper laser levels.

(c) Radiative relaxation out of all other levels to minimize thermal input.

(d) Stimulated emission cross section in the range 10^{-19} -10^{-21} cm^2.

(e) Host properties consistent with high peak and average power operation.

Based on these requirements, several candidates have been identified and are discussed below. In some cases, all the requirements are not met and in some cases sufficient spectroscopic data is unavailable, and choice was made based only on absorption at the excimer lines and the existence of an energy level structure in the ion consistent with low heating. At the present time, the most promising candidate is Tm^{3+}.

3.4.2 Tm^{3+}:YLF

The energy levels of Tm^{3+}:YLF have previously been determined by Jenssen, et al[17]. A partial level diagram is shown in Figure 10. Tm^{3+} absorption at 353 nm is due to the $^3H_6 \rightarrow {}^1D_2$ transition shown in the spectra of Figure 11. The 353 absorption cross section is approximately 6×10^{-22} cm^2. Since 100% Tm^{3+} substitution of Y^{3+} in $LiYF_4$ can be grown ($LiTmF_4$) absorption coefficients as high as approximately 6 cm^{-1} are possible at 353 nm*.

The $^1D_2$ emission occurs in two groups of lines, one corresponding to $^1D_2 \rightarrow {}^3H_4$ transitions (450 nm) and the other to the $^1D_2 \rightarrow {}^3H_6$ transition (360 nm). $^1D_2$ emission in π and σ polarizations is shown in Figures 12 and 13. The peak emission for the $^1D_2 \rightarrow {}^3H_4$ laser transition is at 449.5 nm in the π spectrum and at 451.0 nm in the π spectrum. Tm^{3+} exhibits no absorption from $^3H_6$ at the $^1D_2 - {}^3H_4$ emission line.

The $^1D_2$ fluorescence lifetime was measured by resonant pumping of $^1D_2$ (filtered Xe pulsed lamp with a duration of 1 μs) and detection of the blue fluorescence with narrow band filters. The

* The absorption coefficient for 100% is mentioned only to indicate the range of absorption coefficients possible.

Tm^{3+}:YLF ENERGY LEVELS

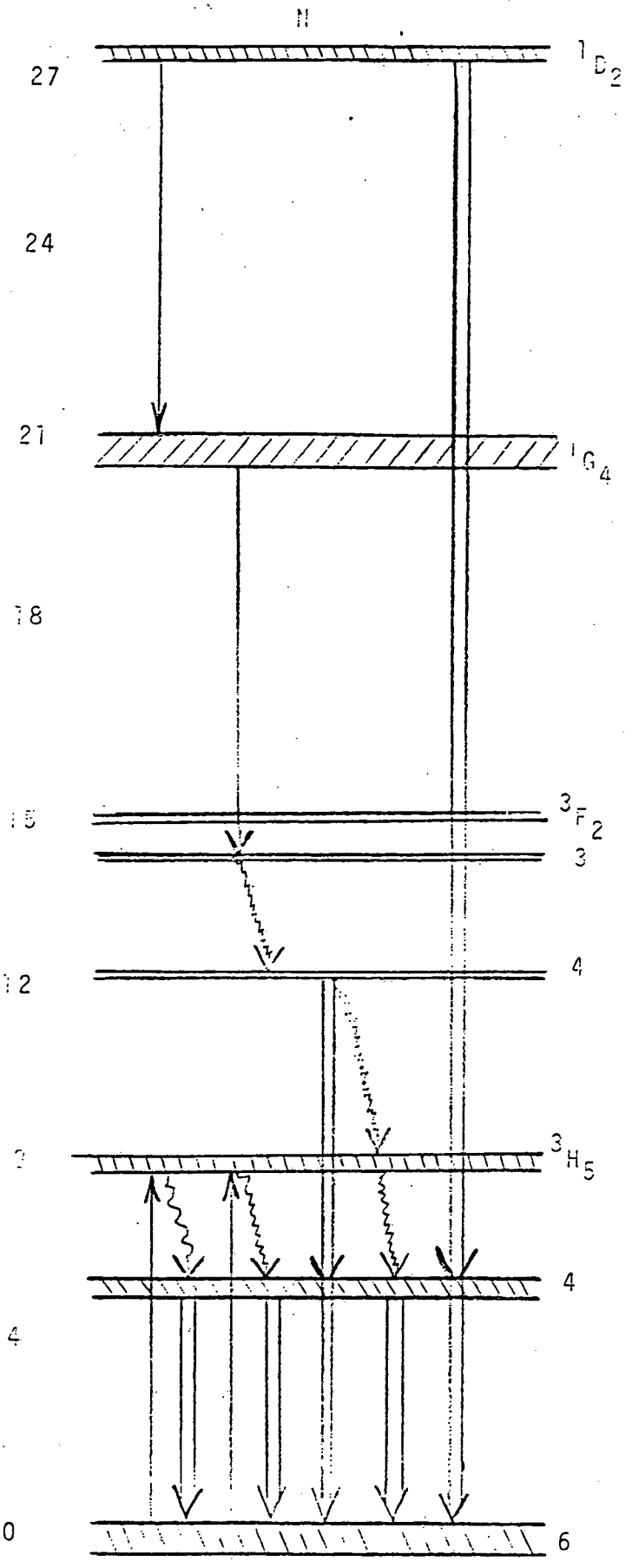

Quenching processes in Tm^{3+}

Quenching by impurities

Multiphonon relaxation

Radiative transition

D-766

Figure 10

ABSORPTION SPECTRA OF Tm:YLF

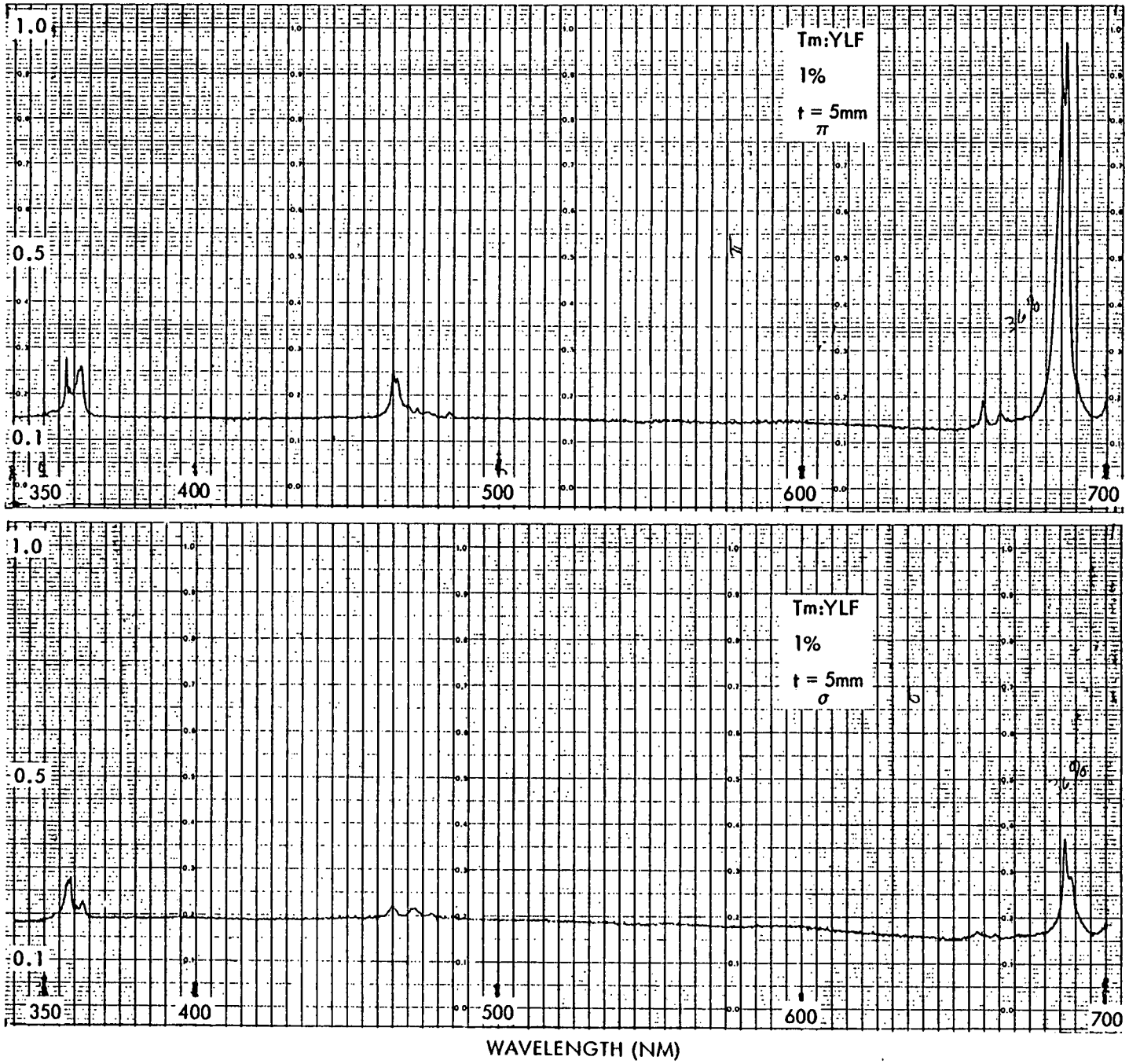

FIGURE 11

D-742

FIGURE 12

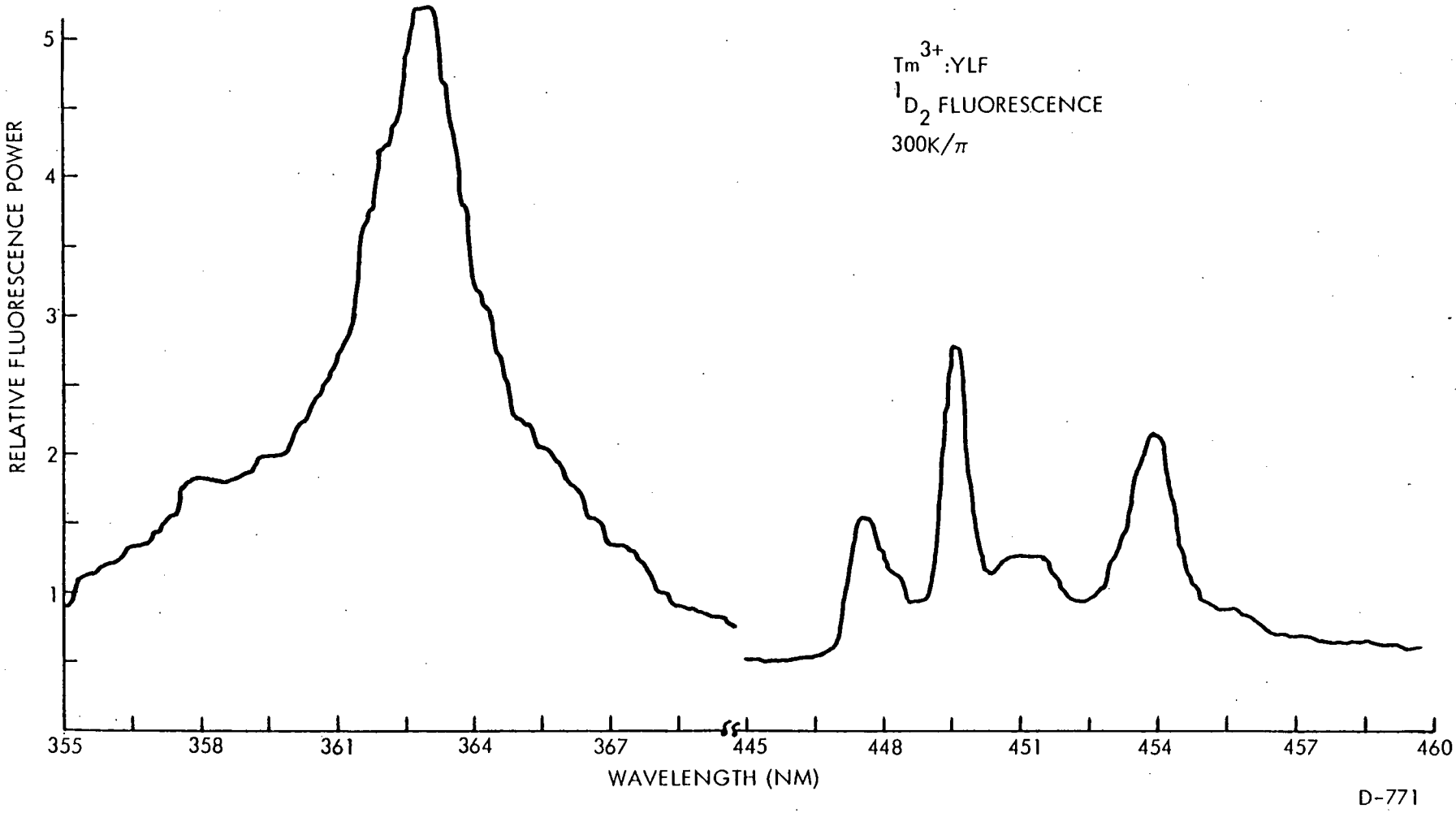

EMISSION SPECTRA OF Tm:YLF (σ)

FIGURE 13

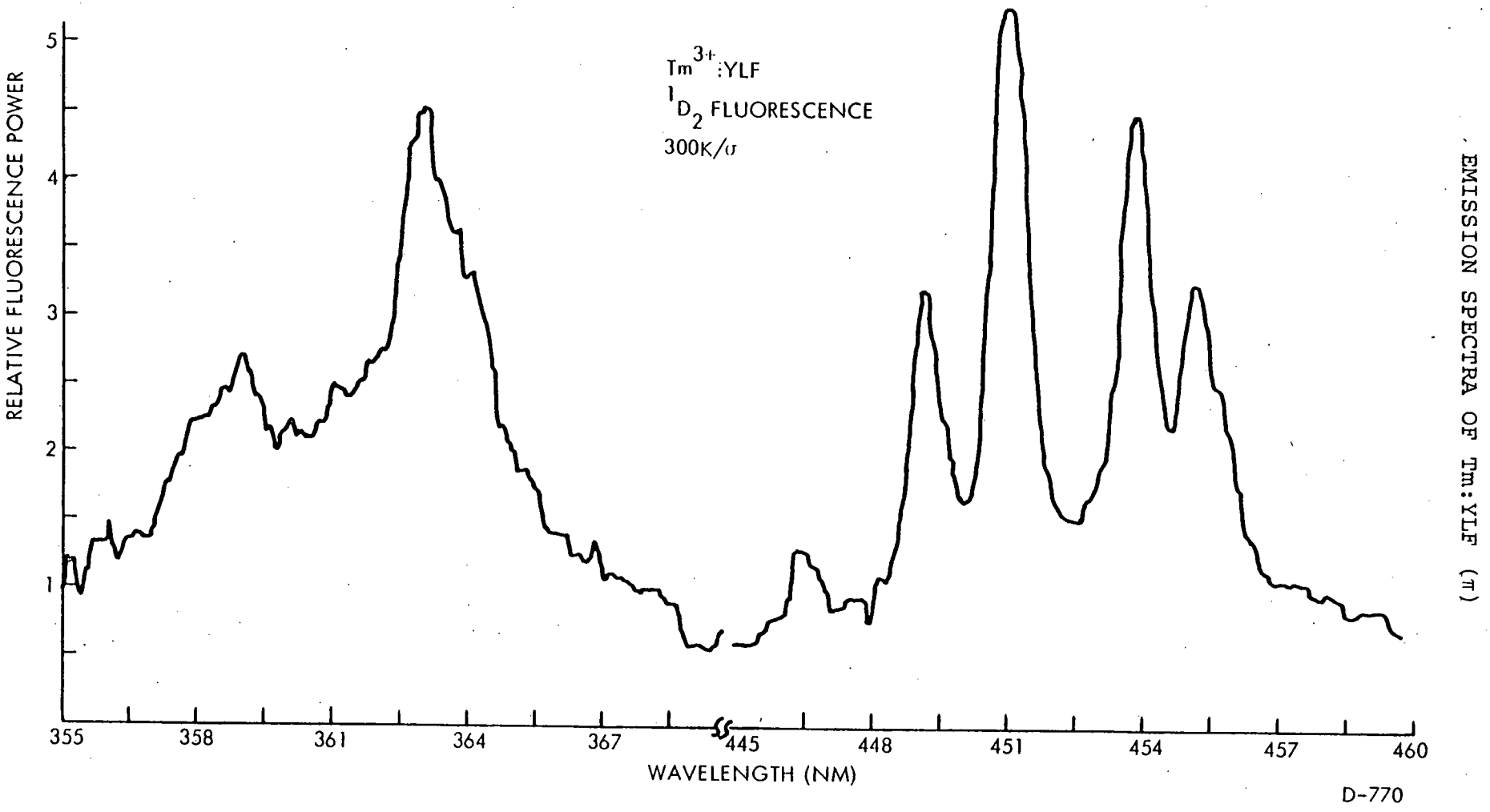

EMISSION SPECTRA OF Tm:YLF (π)

measured $^1D_2$ lifetime in 1% Tm^{3+}:YLF at 300K is 67 μs. Figure 14 shows a photograph of the $^1D_2$ fluorescence decay.

The intra-manifold states involved in these transitions have not been identified with sufficient accuracy to permit an exact determination of the emission cross sections. A preliminary estimate can be made, however, in the following way. The only observed $^1D_2$ fluorescence in a 1% Tm:YLF crystal is $^1D_2 \rightarrow {}^3H_4$ and $^1D_2 \rightarrow {}^3H_6$. If the measured fluorescent lifetime is the radiative lifetime of the $^1D_2$ level, we can obtain the total transition probability for the $^1D_2 \rightarrow {}^3H_4$ transitions from the radiative lifetime and the branching ratio β

$$\beta = \frac{\int_{^3H_4} \lambda I(\lambda) d\lambda}{\int_{^3H_4} \lambda I(\lambda) d\lambda + \int_{^3H_6} \lambda I(\lambda) d\lambda}$$

Where $\int_{\lambda} I(\lambda) d\lambda$ is the total number of photons emitted in the $^1D_2 \rightarrow {}^3H_4$, transitions. From preliminary measurements, β is estimated to be between 0.4 and 0.6. The radiative lifetime for the $^1D_2 \rightarrow {}^3H_4$ transitions is therefore $\frac{1}{\beta} T\,(^1D_2)$ or 110 to 160 μsec. If we now use the formula relating radiative lifetime and stimulated emission cross section for a Lorentzian line with the same effective width as the emission from $^1D_2 \rightarrow {}^3H_4$, we have for the peak cross section:

$$\sigma_p = \frac{\lambda}{4\pi^2 n^2 t \Delta\nu} = 6\text{-}9 \times 10^{-20}\ cm^2$$

This method is used with quite good accuracy for Nd:glasses. For Tm:YLF two things might affect the accuracy. First, the YLF crystal

FIGURE 14

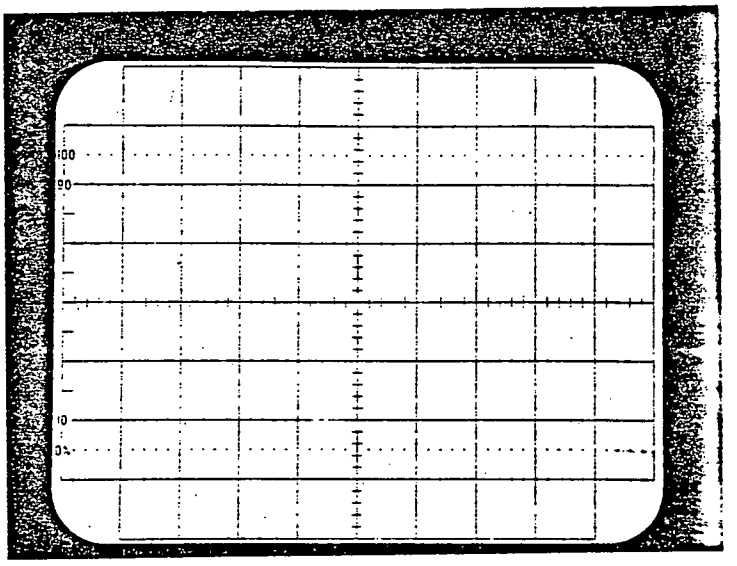

$^1D_2$ FLUORESCENCE DECAY

SUCCESSIVE TRANSFER MODEL FOR THE SENSITIZED EXCITATION OF Tm^{3+} IONS BY NEAR 1 μm RADIATION

FIGURE 15

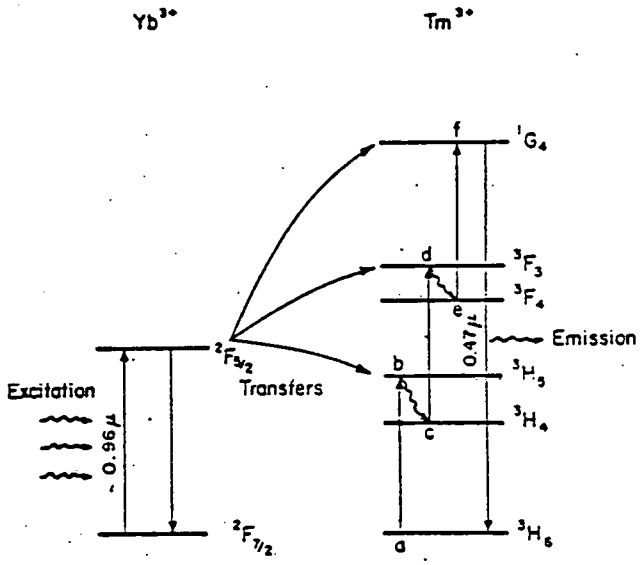

Successive transfer model for the sensitized excitation of Tm^{3+} ions by near 1 μm radiation (after Auzel[4]).

is uniaxial and therefore results in polarized lines and the calculation of the branching ratio should take this into account. Second, the effect of selection rules and degeneracies have not yet been considered. The peak cross section does, however, fall in the desired region for a fusion laser.

A further point of interest is the no $^1G_4$ emission is observed when $^1D_2$ is pumped. In fact, the only transitions observed for $^1D_2$ are to $^3H_4$ and $^3H_6$. This is a very encouraging result as other relaxation modes could result in the generation of substantial heat. Tm^{3+} in YLF may be close to the ideal type II laser.

In low concentrations ($^1D_2$ relaxation 100% radiative), the only heat load is associated with:

Multiplet relaxation
Fluorescence reabsorption
Upconversion

In rare earth ions, excited levels of two ions can interact leaving one ion excited to a higher level (at roughly an energy level corresponding to the sum of the energies of the initial excitations.) Upconversion in Tm^{3+} has been observed by many workers [18] but there are no known reports of such processes with only $^3H_4$ populated. Typical upconversion processes in Tm^{3+}, shown in Figure 15, require the presence of 1 μm excitation generally obtained by energy transfer from Yb^{3+}.

In lightly doped Tm^{3+} resonantly pumped to $^1D_2$, the only excited levels appreciably populated by the $^1D_2$ decay are $^3H_4$ and $^3H_6$. A possible mechanism under these conditions is an ion pair process involving two Tm^{3+} ions initially excited to $^3H_4$ relaxing with one ion in $^3H_6$ and the other in $^3H_4$. Such a process is not resonant requiring about 500 cm^{-1} phonons for energy conversation and is not expected to be significant. At higher concentration where the $^1D_2$ relaxation is more complex, upconversion might be more likely.

However, even under ideal condition (Yb^{3+} sensitized) upconversion efficiencies in Tm^{3+} are only the order of 10^{-2} (19).

The heat load due to fluorescence reabsorption is equally difficult to estimate accurately. In dilute Tm^{3+} the only fluorescence is $^3H_4$ - $^3H_6$. There is significant overlap between the absorption to and emission from $^3H_4$. At high concentrations where the $^3H_4$ absorption is moderate thermal loading due to fluorescence reabsorption might be significant.

Neglecting upconversion and fluorescence reabsorption the heat load of a lightly doped Tm^{3+}:YLF amplifier is estimated in the following way. In XeF pumped operation, the only levels involved are $^1D_2$, $^3H_4$ and $^3H_6$ whose multiplet splittings are (approximately) 400, 200, and 100 cm respectively, a total of 700 cm. The worst case heat load for intramanifold relaxation is the extent of each manifold. So each stored 450 nm (22,220 cm^{-1}) electron will relax with 700 cm of heat, a heat loading of about 3%. At higher concentrations where quenching of the $^1D_2$ fluorescence may become significant the thermal loading can be much higher.

3.4.3 Nd^{3+}:YLF

Figure 16 shows the absorption spectrum of Nd:YLF in and σ polarizations in the region XeF emission. Absorption at 353 nm is strong and would be accomplished by very rapid multiphonon relaxation to 358 nm which would serve as an upper laser level for a variety of possible transitions. The absorption cross section is $\sigma_A = 1.4 \times 10^{-20}$ cm^2 at 353 nm. The specific levels involved are believed to be the ^4D_J multiplets.

Figure 17 shows the Nd^{3+} emission from this multiplet obtained by pumping the crystal with narrow band radiation between 350-360 nm. The emission lines observed are tentatively identified as:

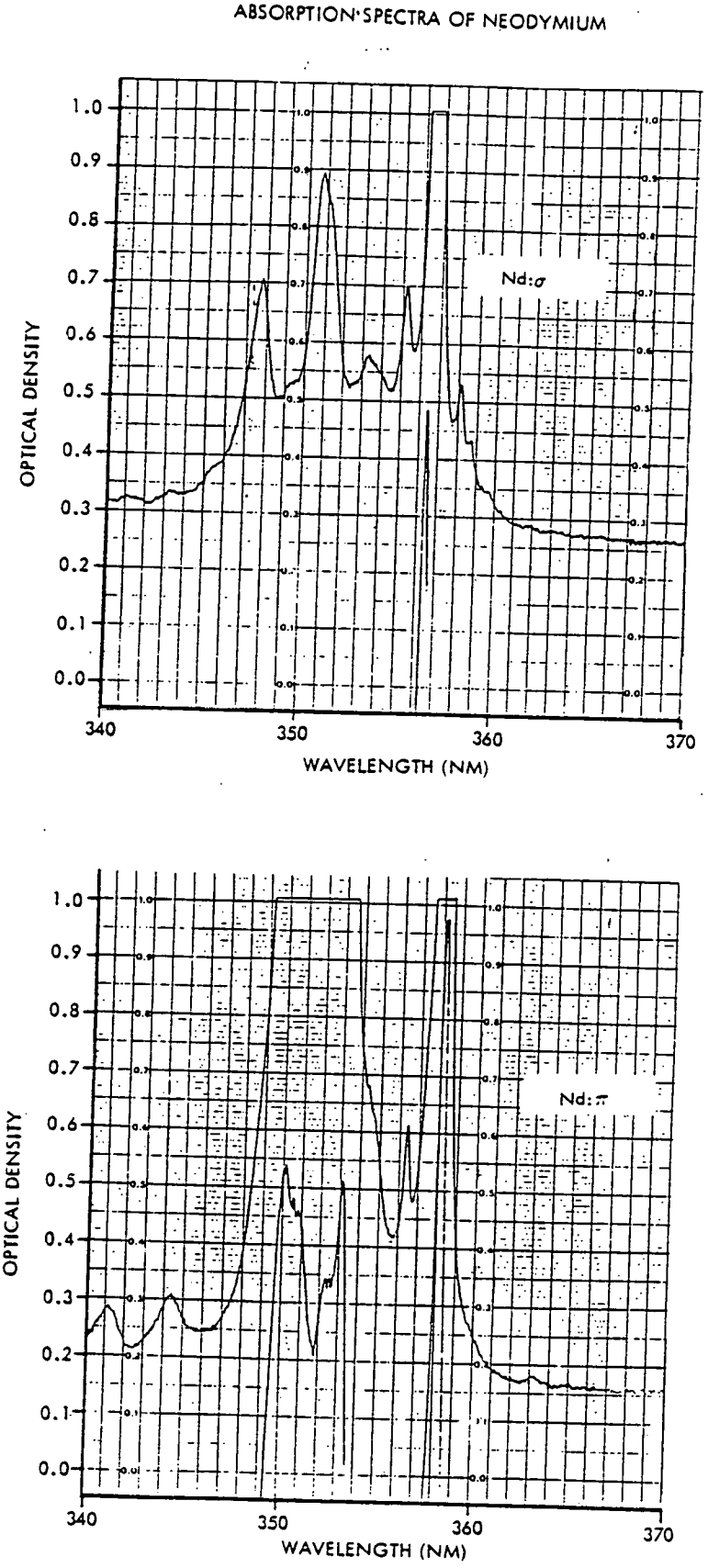
ABSORPTION SPECTRA OF NEODYMIUM
OPTICAL DENSITY
1.0
0.9
0.8
0.7
0.6
0.5
0.4
0.3
0.2
0.1
0.0
Nd:σ
340
350
360
370
WAVELENGTH (NM)
OPTICAL DENSITY
Nd:π
WAVELENGTH (NM)

FIGURE 16

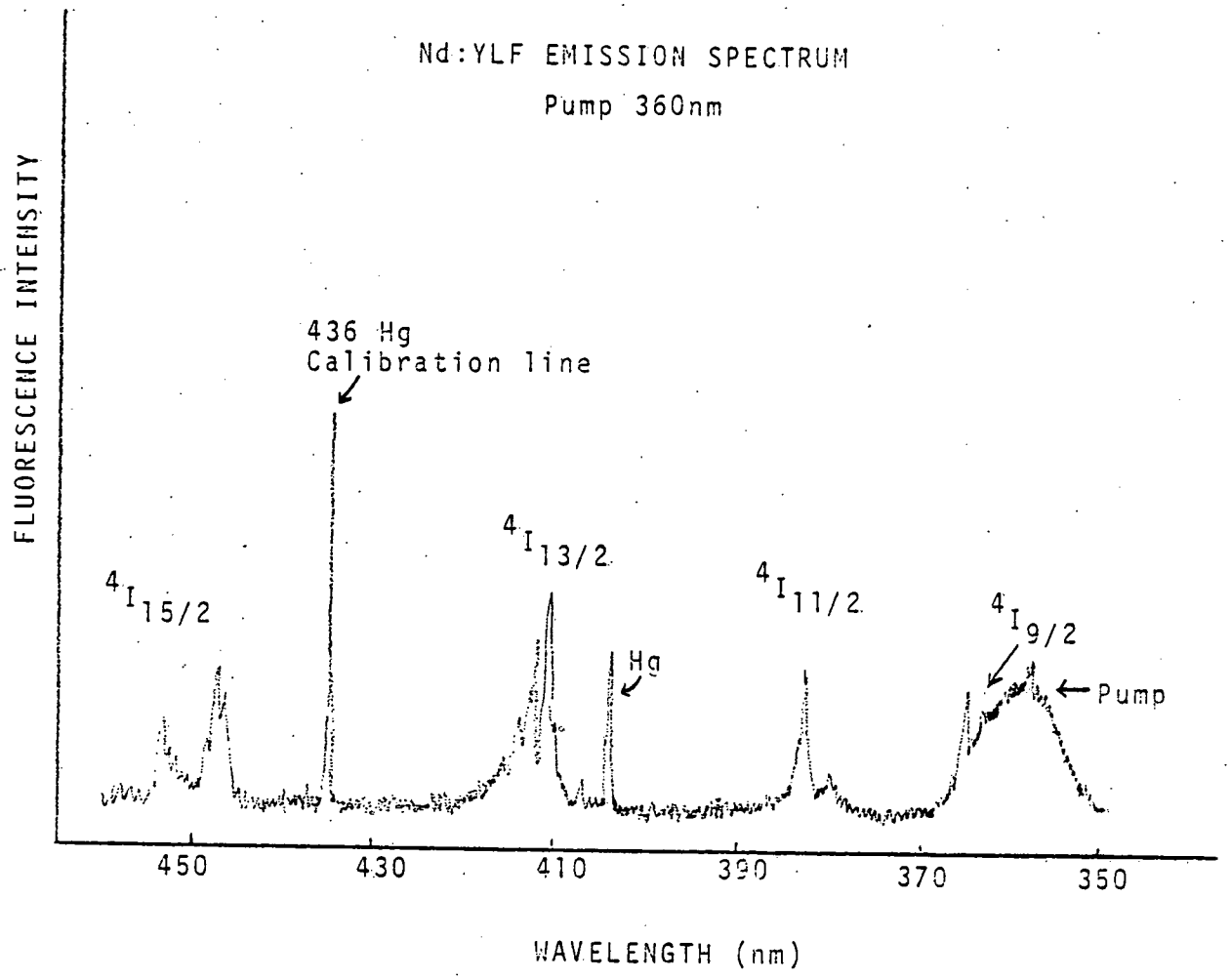

FIGURE 17

D-765

$^4D_{3/2}$	$^4I_{9/2}$	(364 nm)
$^4D_{3/2}$	$^4I_{11/2}$	(382 nm)
$^4D_{3/2}$	$^4I_{13/2}$	(410 nm)
$^4D_{3/2}$	$^4I_{15/2}$	(450 nm)

All these transitions are generically type III. Relaxation from all the "I" multiplets would be primarily phonon assisted. For minimum heat loading, the best choices are the 364 and 382 nm transitions, the former is a 3 level transition and would have the lowest heat load. Quantitive estimates of the heat loading require measurement of the $^4D_{3/2}$ lifetime, branching ratios, and non-radiative decay rate. These measurements are currently in progress. The minimum loading possible, assuming 100% radiative relaxation of $^4D_{3/2}$ to $^4I_{11/2}$ is about 3% or 8% respectively. This is a very optimistic assumption, however.

3.4.4 Ho^{3+}:YLF

Figure 18 shows the absorption spectrum of Ho^{3+}:YLF in the region of KrF emission. At 249, the absorption is weak, the absorption cross section is only 4×10^{-22} cm^2 which for 100% Ho substitution will result in an absorption coefficient of 2.2 cm^{-1}. At the present time, very little is known about this transition and work is ongoing to characterize the parameters of this multiplet which absorbs at 249 nm.

Identification of this transition as a candidate is speculative at this point. It was selected because of the absorption at 249 and because of the anticipated slow multiphonon relaxation rate. A multiphonon relaxation rate slow compared to the radiative rate is anticipated because of the large energy gap to the next lower

ABSORPTION SPECTRA OF HOLMIUM

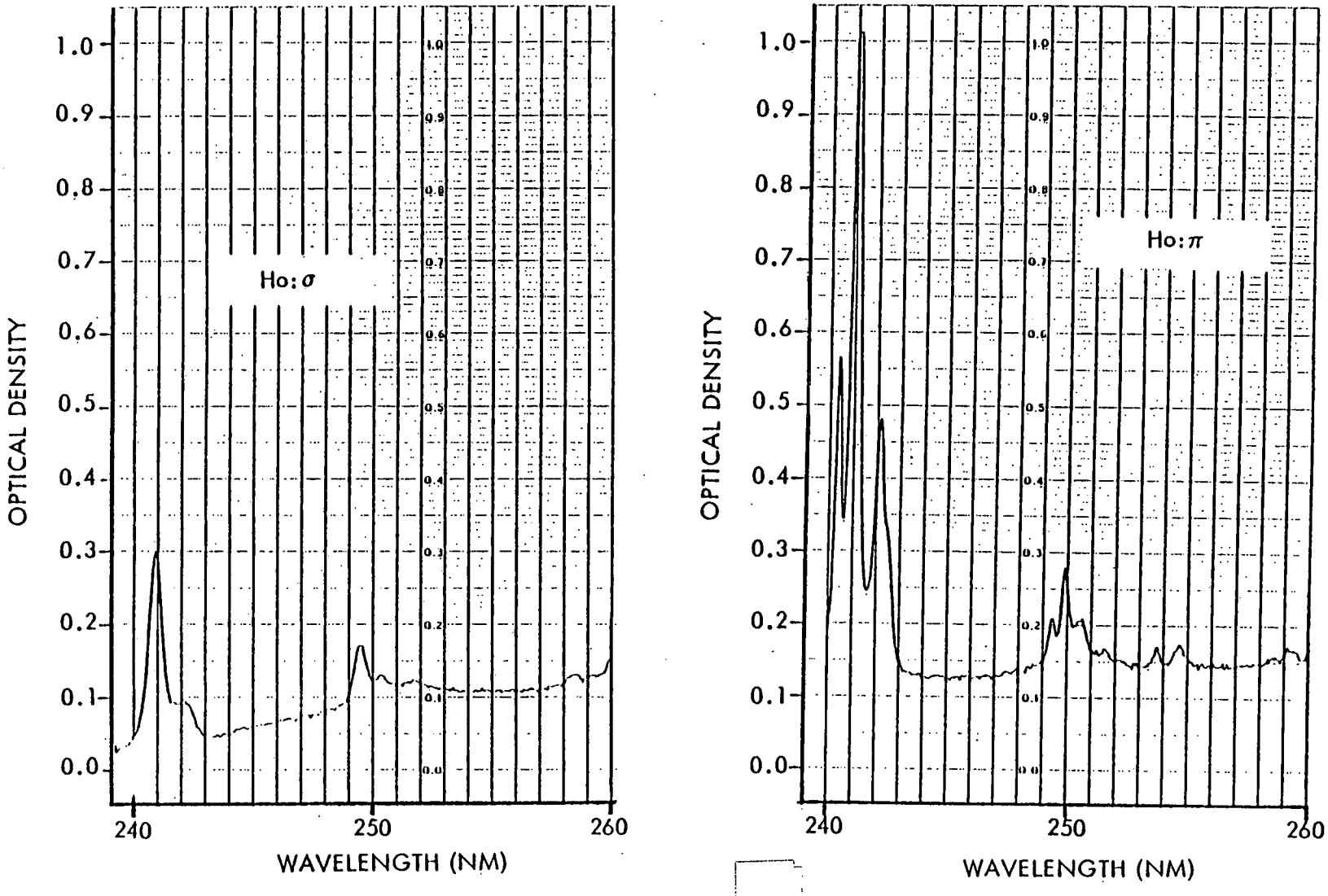

FIGURE 18

D-773

lying multiplet. Spectroscopic measurements are currently underway to characterize the parameters of this multiplet; complete characterization may require a KrF pump.

3.4.5 Divalent Ions

Divalent rare earth ions tend to have broad (allowed) absorption bands in the visible, near ultra-violet regions. Furthermore, some of the divalent ions (Eu^{2+}, Yb^{2+}, and Sm^{2+}) are stable in CaF_2.[20] Specific examples are cited below:

Eu^{2+}

Eu^{2+} exhibits [21] strong absorption at 351 and 193 nm in CaF_2, SrF_2, BaF_2 and emission in the blue near 413 nm. However, at room temperature, the emission is quenched. This transition is reported[21] to be electric dipole with a lifetime of 0.7 μs. As a result the emission cross section might be much too large for this application.

$Yb^{2+}:CaF_2$

Feofilov [22] reports long lived yellow fluorescence in $Yb^{2+}CaF_2$ crystals at low temperatures. The long lifetime 200 μs indicates a cross section comparable to Re^{3+} ions, viz, 10^{-19} -10^{-20} cm^2. Absorption is broadband for $\lambda<400$ nm. The heat loading could be quite small as there is no terminal level relaxation (3 level laser). Sufficient data is not available.

3.4.6 f-d Transitions

The $4f^{n-1}5d$ levels of trivalent rare earths are generally located at energies of 50,000 cm^{-1} above the $4f^n$ ground level. Transitions between $4f^{n-1}5d$ involve a change in the orbital quantum number and as a result are generally allowed electric dipole transitions. Furthermore, d bands exhibit broad absorption as they are not shielded

from the local environment as is the case with f^n-f^n transitions. However, f-d transitions are probably too strong (in emission) for adequate energy storage, typical emission cross sections being 1-5 x 10^{18} cm^2.

For energy storage applications, it may be reasonable to consider a system which absorbs via an f-d transition accompanied by rapid multiphonon relaxation to a metastable f level which can be utilized as the upper laser level. The advantage of this type of system is the absorption overlap with excimer lines (ArF, KrF). At the present time, the only known candidate is Pr^{3+} described below.

Pr^{3+}

Pr^{3+} LaF_3 absorbs at 193 nm (f-d transition). This is followed by rapid multiphonon relaxation to ^1S_o. This level fluoresces to several lower lying levels; the transitions from ^1S_o are f-f transitions and the S level lifetime is ~1 s. The strongest emission lines are to $^1I_6$ (λ= 390), $^1G_4$ (λ= 270), and $^3F_4$ (λ= 250). (23)

This is a type IIa and type IIb system. If the predominant emission is to 250 (via stimulated emission) then the heat load would be about 22%*. This can only be diminished by forcing the system to lase at shorter wavelength transitions. If, for example, the terminal level were $^3H_5$, the wavelength would be about 200 nm and the heat load only about 3%. This, of course, neglects the heat load associated with other spontaneous emission decay routes.

The cross section of the ^1S_o-$^3H_5$ transition is not known but it is considerably weaker in CaF_3 than the $^1G_4$, $^3F_4$, and $^1I_6$ transitions. Another possibility for this system is a terminal level of $^1I_6$ or $^1G_4$. In the former case, $^1I_6$ relaxes to ^3P_o which emits by fluorescence. This could result in a heat load of only a few percent. The same is true for $^1D_2$. $^3F_4$, however, relaxes by multiphonon relaxation and its heat load is rather high.

*It is assumed that $^3F_4$ relaxes to $^3H_4$ by multiphonon relaxation.

The use of f-d absorption transitions may result in prohibitively low active ion concentrations when large (thick) samples such as amplifiers are utilized. For the moment, such transitions are included in this survey for completeness.

3.4.7 Ruby

Cr^{3+} in Al_2O_3 exhibits many desirable properties as a high power laser material. Specific properties of interest are:[24]

(a) High Thermal Conductivity

k = 0.4 watts/cm-K (300K)
k = 20 watts/cm-K (77K)

(b) Tunable Emission Cross Section (Temperature)

$\sigma = 2.5 \times 10^{-20}$ cm^2 (300K)
$\sigma \simeq 2 \times 10^{-18}$ cm^2 (77K)

(c) Long Storage Time

T = 2.5 ms (upper laser level)

(d) High Damage Resistance

>10J/cm^2

Since one of the key issues for high power solid state lasers is their capacity to dissipate the thermal input, the excellent thermal-mechanical properties of ruby alone merit close consideration of this material. (At 77K ruby exhibits a higher thermal conductivity than copper.)

The ruby level structure (Figure 19) is such that the dominant relaxation mode of the upper laser level is via radiative transitions to the ground state, unlike the case of rare earth ions where many alternate decay modes are available. This means that the thermal input to a ruby system will be dominated by pump band -

RUBY ABSORPTION SPECTRUM

&

ENERGY LEVELS

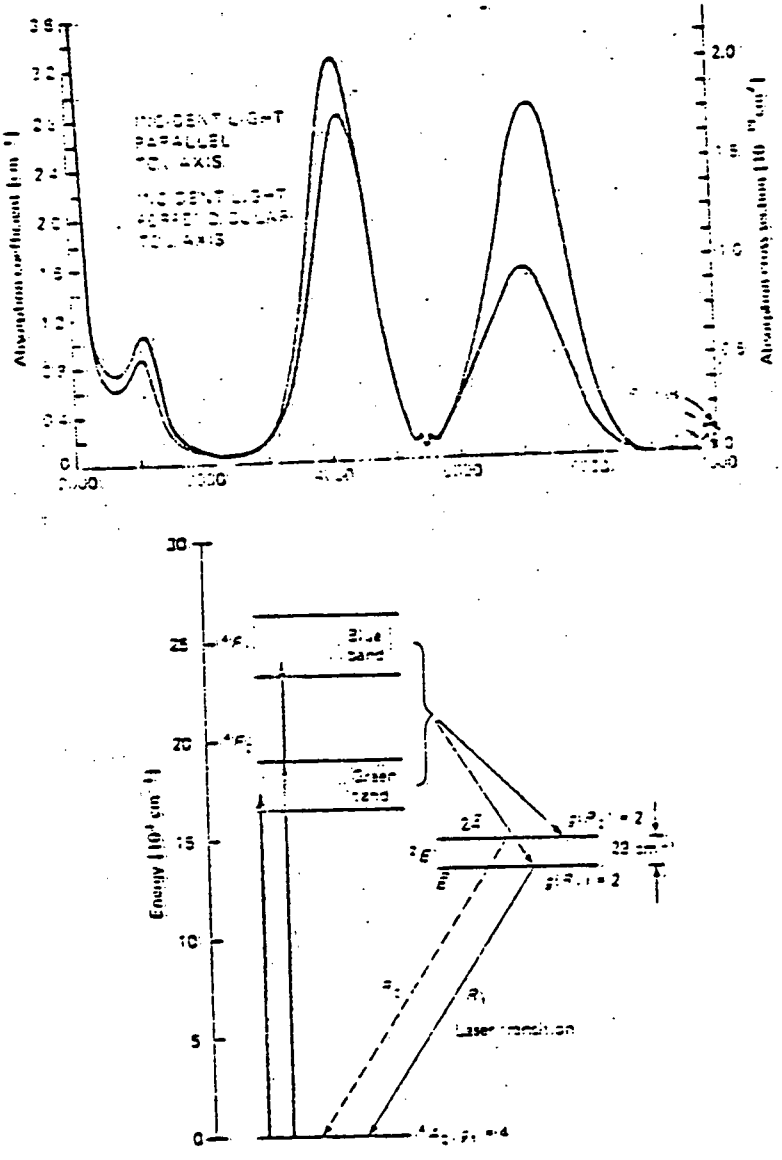

FIGURE 19

metastable level relaxation.

Unfortunately, the thermal loading with a XeF pump is very high due to the large gap between the pump level and the upper laser level. Furthermore, because ruby is a true 3 level laser, only 50% of the stored energy can be extracted, the remainder will decay by spontaneous emission. This results in a thermal input of 2 joules of extractable energy assuming pure spontaneous decay of the remainder of the stored population with no fluorescence reabsorption.

In general, if K represents the ratio of pump photon energy to the energy of the stored photon, then the heat input from pump to metastable relaxation is (k - 1) hv. The stored energy is simply hv; but the extractable energy is hv/2. Thus, the fractional loading for any 3 level laser is 2 (k - 1).

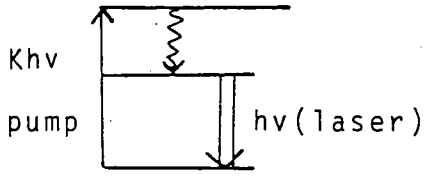

Pump energy = khv
Stored energy = hv
Extractable energy = hv/2

Fractional loading, Q = 2(k-1)

A further difficulty with ruby is the optical quality of available material may not be sufficiently high. [25] Both difficulties might be overcome by the development of a pump (HgCl?) in the region of 550 nm. With a 550 nm pump, $k \simeq 1.26$ and $Q = 0.5$, viz a 50% heat load. Furthermore, the high absorption coefficient of ruby in this region ($\sim 3\ cm^{-1}$) would permit the use of much more dilute Cr^{3+} concentrations than the standard (0.05% Cr^{3+}) doping and substantially ease the problems of growth of sufficiently high quality material. Ruby will be particularly attractive if efficient pumps in the 550 nm region are developed.

3.4.8 Host Material

Choice of a host material is based on several considerations including the effects of the host on spectroscopic parameters of the dopant ion, the scaleability of the material growth to large apertures, the non-linear index of the material, the ultra-violet absorption edge, and the resistance of the material to laser damage. The most promising materials identified are Tm^{3+} and Ho^{3+} doped YLF. At the present time, YLF as a host for these ions appear very attractive for the following reasons.

(a) Spectroscopic Properties.

YLF has a natural rare earth site which permits arbitrary amounts of Tm^{3+} and Ho^{3+} substitution for Y^{3+} without significantly affecting crystalline quality, fluorescence line width or ease of growth . The multiphonon relaxation rate in YLF is lower than in most laser hosts. This results in a lower heat input due to non-radiative decay routes. In the case of Tm^{3+} the $^1D_2$ absorption and emission cross section are somewhat higher in YLF than in glasses or cubic hosts because YLF lacks inversion symmetry.

(b) Ultraviolet Edge and Laser and Ultraviolet Damage Resistance

Currently the most efficient excimer lasers operate in the ultraviolet (ArF-193, KrF-249, KeF-353 nm). For resonant pumping with these sources, a material with very high ultraviolet damage resistance is needed, and transparency at twice the pump energy is desirably to minimize the possibility of two-photon absorption by the host. Table III shows measured transmission of YLF in the ultra-violet together with the excimer lines and the doubled wavelength. It appears that two photon absorption in YLF may not be significant for XeF and KrF pumps, but that use of ArF may not be practical.

The laser damage threshold of YLF at 1060 nm has recently been measured [26] and the results are shown in Table IV. Of all

TABLE III

SHORT WAVELENGTH CUTOFF OF YLF

MEASURED TRANSMISSION (2mm THICK)*

Undoped $LiYF_4$ Grown by Sanders

ENERGY	WAVELENGTH	TRANSMISSION
eV	nm	%
10.0	124	55
10.5	118	5

EXCIMER LASERS				
	OUTPUT		TWO PHOTON	
	ENERGY	WAVELENGTH	ENERGY	WAVELENGTH
	eV	nm	eV	nm
XeF	3.54	350	7.08	175
Krf	4.98	249	9.95	125
ArF	6.43	193	12.92	96

*Measured by V. Rehn, NWC, China Lake

TABLE IV

BULK LASER DAMAGE THRESHOLDS UNDER Q-SWITCHED 1.06 μm IRRADIATION*

(40 μm focal spot size, 4.65 ns pulsewidth FWHM)

Material	Power Density (GW/cm^2)	Electric Field (MV/cm)	Relative Power Density (to Nd:YAG)
Nd:YLF	18.9	2.21	1.87
Nd:ED2.3	16.9	2.2	1.67
Nd:BEL (E//y)	10.5	1.4	1.04
Nd:YAG	10.1	1.45	1.00
Nd:BEL (E//z)	9.33	1.33	0.92
NaCl	7.64	1.39	0.76
$Nd:YVO_4$	<6.43	<1.14	<0.64
Nd:GGG	5.56	1.08	0.55

*M. Birnbaum, L. DeShazer, "Engineering Design of Repetitively Q-switched Solid State Lasers for Precision Ranging Application" Contract NASA-23698

the laser host materials measured YLF exhibits the highest damage threshold, nearly 19 x 10^9 w/cm^2, a factor of 1.8 times higher than Nd:YAG. For driver applications, energy densities the order of 10J/cm^2 is 1 ns, or 1 x 10^9 w/cm^2, are anticipated. It appears that YLF has a comfortable safety margin.

The ultraviolet damage resistance of YLF is known to be very high, but there is no quantitative data. YLF laser rods are routinely pumped by high pressure, high current density Xe flashlamps with clear fused quartz envelopes. Furthermore, Tb^{3+}:YLF crystals have been pumped with unfiltered dye laser flashlamps operated at 50J/inch in 1 s without any evidence of ultraviolet induced damage.[28] Most other laser hosts (certainly most oxide laser hosts) would exhibit some form of damage under these pumping conditions.

(c) Physical Properties

The non-linear index of refraction of YLF is 0.6 x 10^{-13} esu [29], which is adequately low for driver applications. Growth of YLF is at a comparatively low temperature (820C) with low thermal gradients resulting in very low strain and high optical quality. Other physical properties of this host materials shown in Table V.

(d) Scaleability

At the present time, the largest boules of YLF which have been grown are 3.5 cm diameter by 15 cm in length. Driver applications will require much larger apertures. Without modification of the growth technique (VIZ with Czochralski growth) or current apparatus (Sanders automated growth facility) it is anticipated that 10 cm diameter boules can be grown. Using Czochralski growth with modified apparatus, diameters up to 20 cm appear technically feasible. There is no known fundamental limitation to scale of this growth technique to arbitrarily large diameters. Another promising technique for growth of much larger crystals is a modified Bridgeman technique such as Bottom Seeded Solution Growth. Bridgeman growth has produced

TABLE V

MATERIAL AND OPTICAL PROPERTIES

YLF ($LiYF_4$)

and

YAG ($Y_3Al_5O_{12}$)

	YLF	YAG
MECHANICAL		
Density (gm/cm^3)	5.07 ($\alpha\beta$YLF)	4.47
Hardness (Mohs)	4-5	8.5
Elastic Modulus (N/m^2)	7.5×10^{10}	33.3×10^{10}
Strength (N/m^2)	3.3×10^{7}	
THERMAL (300°K)		
Thermal Conductivity W/cm-°K	0.06	0.13
Thermal Expansion Coefficient - $°C^{-1}$	a axis : 13×10^{-6} c axis : 8×10^{-6}	6.9×10^{-6}
OPTICAL		
Index of Refraction $\lambda = 0.6$ µm	$n_o = 1.443$ $n_e = 1.464$	1.8347
UV Absorption	<0.2 µm	~0.38 µm
CRYSTALLINE STRUCTURE	Tetragonal (Scheelite)	Cubic (Garnet)

SANDERS ASSOCIATES, INC.

CaF_2 crystals greater than 25 cm diameter. For growth of YLF, these techniques are applicable. The complicating factors are that YLF is incongruently melting and is uniaxial. Neither of these factors pose fundamental limitation on aperture, rather engineering challenges. An important advantage of this material for scaling the growth is its low growth temperature (820°C) in contrast to CaF_2 (1360°C) and Sapphire (2050°C).

3.4.9 Summary

Candidate transitions are summarized in Table VI. This is a preliminary tabulation, work is ongoing to identify others, particularly f-d absorption transitions in Re^{3+} ions.

In the absence of data on oscillator strengths, multi-phonon relaxation rates, and fluorescence branching ratios the estimates of the thermal loading must be considered tentative. The thermal loads estimated in Table VI are optimistic representing rather ideal conditions.

Of all the candidates examined to date, Tm^{3+}:YLF appears most attractice. The emission cross section is suitable for high power operation; the fluorescence lifetime is adequate for energy storage; the decay mode out of the upper laser level appears to be nearly 100% radiative; and the thermal load very low. Ho^{3+} is not as attractive, but the superior performance of KrF compared to XeF merits investigation of this as well as other possible KrF down-converters.

TABLE VI HIGH POWER LASER CANDIDATES

Ion/Host	Pump Transition/Pump	Laser Transition (λ-nm)	Fractional Heat Load+	Remarks
Tm^{3+}/YLF	$^3H_6$ - $^1D_2$/XeF	$^1D_2$ - $^3H_4$ (450)	3%	$^1D_2$ emission appears purely radiative $\sigma \cong$ 6-9 x 10^{-20} cm^2
Nd^{3+}/YLF	$^4I_{9/2}$ - ^4D_J/XeF	$^4D_{3/2}$ - $^4I_{9/2}$ (364)	3%	Heat load could be much higher depending on multiphonon relaxation rate out of $^4D_{2/3}$
		$^4D_{3/2}$ - $^4I_{11/2}$ (382)	8%	
Ho^{3+}/YLF	Absorption transmission not identified (KrF)	multiple transitions possible	?	Moderate 249 absorption in Ho:YLF, emission unknown
Eu^{2+}/CaF_2	Broad band absorption at λ<400nm ArF, KrF, XeF	λ=413, d-f(?)	depends on pump, ~16% for XeF	No fluorescence reab sorption but emission cross section may be too high. Should be stable in CaF_2
Yb^{2+}/CaF_2	Broadband absorption λ<400nm	Yellow emission in CaF_2	~20%	No fluorescence reabsorption. Stable in CaF_2.
Pr^{3+}/LaF_3	f-d absorption/ArF	^1S_o - $^3H_5$ (200 nm)	3%	LaF_3, results in other fluorides not known Lifetime ~1 μs.
		^1S_o - $^3F_4$ (250)	22%	
		^1S_o - $^1I_6$ (393)	few %	
		^1S_o - $^1G_4$ (270)	few %	
Cr^{3+}/Al_2O_3	$^4A_2$ - $^4F_2$/?550nm	^2E - $^4A_2$	~50%	Low Cr^{3+} doping. High heat load but excellent thermal-mechanical properties

4.0 CONCLUSIONS

Nd:YLF laser rods fabricated from single crystal boules grown for this program have been mode locked in Q switched resonators. The neodymium concentration in the rods, 1% is comparable to Nd:YAG. This laser material has been transitioned to a commercial product.

Small samples of KTb_3F_{10} have been grown and employed to develop a partial phase diagram. The measured magneto-optical properties of KTb_3F_{10} has resulted in a figure of merit 4.3 times that of FR-5 glass.

Initial investigation of additional faraday rotator materials, specifically $RbTb_3F_{10}$ and the $KF\text{-}CeF_3$ system has begun.

Work has begun in the development of crystal growth techniques to grow large fluoride crystals. Specifically, the hot zone assembly has been designed and fabricated. A seed rod with increased rigidity has been fabricated.

The investigation of rare gas halide pumped solid state lasers has predicted specific cases in which high efficiencies with very low heat deposition is likely. The best candidate system appear to be XeF pumped Nd^{+3}:YLF, XeF pumped Tm^{+3}:YLF, and KrF pumped Ho^{+3}:YLF. Heating loading in all cases is estimated as 10% or less of stored energy. The transitions of the above systems have been characterized, and the stimulated emission cross-section and related data has been determined.

REFERENCES

1. J. Zimmerman, W. Know, W. Seka, "Oscillators for Phosphate Glass Laser Systems", Proc. Topical Meeting on Inertial Confinement Fusion, San Diego, February 1978.

2. D. Kuizenga, Lawrence Livermore Labs, Private Communication.

3. J.C. Guyot, Centre de Recherches de la CGE, Private Communication.

4. S.E. Stokowski, et al., "Fluorophosphate Glass for Fusion Lasers", Proc. Topical Meeting on Inertial Confinement Fusion, San Diego, February 1978.

5. Wolf Seka, University of Rochester, Private Communication.

6. John McMahon, Naval Research Lab, Private Communication.

7. Marvin Weber, Lawrence Livermore Laboratory, University of California, Private Communication.

8. A. Vedrine, R. Boutonnet, R. Sabatier, J-C Cousseins, Bull Soc. Chim., France, 446 (1975).

9. A. De Kozak and M. Samouel, Rev. Chim. Min 14, 93 (1977)

10. J.W. Pierce, J. Y-P Hong and D. Gabbe, "Structure and Growth of KEr_3F_{10} presented by ACS meeting, August 1974.

11. M.P. Borzenkova, G.N. Kuznetsova, and A.V. Novoselova, 120 Akad, Nauk-SSSR, Neorg, Mat. 7 (2) 242-7, 1971.

12. M. Labeau, Y Le Fur, and S. Aleonard, "Phases de Structure du Type Fluorine dans le Systeme $KF'ErF_3$", J. Sol. State, Chem 10, 282 (1974).

13. Charles J. Barton, L.O. GilPatrick, George D. Brunton, David Hsu, and Herbert Insley, "Phase relations in the system $KF-CeF_3$" J. Inorg, Nucl. Chem 33, 325 (1971).

14. Rober Wilson, Varion Associates Private Communication.

15. C.D. Brandle, J. of Applied Physics 49 (3) March 1978 P. 1855.

REFERENCES (CONT'D)

16. G.D. Baldwin, AFAL-TR-72-334 (September 1972).

17. H.P. Jenssen, et al , Phys. Rev. B., 11, No 1, 92 (1975).

18. F. Auzel, Proc. IEEE 61, No. 6, 758 (1973).

19. J.E. Geusic, et al., J. Appl. Phys. 42, No. 5, 1958 (1971).

20. T. Mueller, Inorganic Chemistry, P503 (New York, Wiley, 1952).

21. A.A. Kapyanskii & P.P. Feofilov, Optics & Spectros (1962).

22. P.P. Feofilou, Optics & Spectros 12, 493 (1962).

23. L.R. Elias, et al., Phys Rev. B, V8. No. 11, 4989 (1973).

24. See for example, W. Koechner, "Solid State Laser Engineering", Springer-Verlag, New York, 1976.

25. J.L. Emmet, Lawrence Livermore Labs, Private Communication.

26. M. Birnbaum, L.G. DeShazer, "Engineering Design of Repetitively Q-switches Solid State Lasers for Precision Ranging Applications" Contract NASA-23698.

27. E.P. Chicklis, et al., "Er·YLF Laser Development", AFAL-TR-75-64, Part II, July 1976.

28. H.P. Jenssen, et al., "Laser Emission at 5445A in Tb^{3+}. YLF., CLEA, Washington, D.C. May 1973.

29. D. Milam, M.J. Weber, and A.J. Glass., "Nonlinear Refractive Index of Fluoride Crystals", Appl. Phys. Lett 31 (12), P822-825, (1977).